

Review

# An Overview of Coacervates: The Special Disperse State of Amphiphilic and Polymeric Materials in Solution

Satya Priya Moulik <sup>1</sup>, Animesh Kumar Rakshit <sup>2</sup>, Animesh Pan <sup>3,\*</sup> and Bappaditya Naskar <sup>4,\*</sup>

<sup>1</sup> Centre for Surface Science, Department of Chemistry, Jadavpur University, Kolkata 700032, India

<sup>2</sup> Indian Society for Surface Science & Technology, Department of Chemistry, Jadavpur University, Kolkata 700032, India

<sup>3</sup> Department of Chemical Engineering, University of Rhode Island, South Kingston, RI 02881, USA

<sup>4</sup> Department of Chemistry, Sundarban Hazi Desarat College, University of Calcutta, Pathankhali 743611, India

\* Correspondence: animeshpan555@gmail.com (A.P.); bappadityanaskar25@yahoo.com (B.N.)

**Abstract:** Individual amphiphiles, polymers, and colloidal dispersions influenced by temperature, pH, and environmental conditions or interactions between their oppositely charged pairs in solvent medium often produce solvent-rich and solvent-poor phases in the system. The solvent-poor denser phase found either on the top or the bottom of the system is called coacervate. Coacervates have immense applications in various technological fields. This review comprises a concise introduction, focusing on the types of coacervates, and the influence of different factors in their formation, structures, and stability. In addition, their physicochemical properties, thermodynamics of formation, and uses and multifarious applications are also concisely presented and discussed.

**Keywords:** polyelectrolytes; polymers; surfactants; protein; peptide; coacervates; applications

**Citation:** Moulik, S.P.; Rakshit, A.K.; Pan, A.; Naskar, B. An Overview of Coacervates: The Special Disperse State of Amphiphilic and Polymeric Materials in Solution. *Colloids Interfaces* **2022**, *6*, 45. <https://doi.org/10.3390/colloids6030045>

Academic Editors: Reinhard Miller

Received: 19 July 2022

Accepted: 29 August 2022

Published: 6 September 2022

**Publisher's Note:** MDPI stays neutral with regard to jurisdictional claims in published maps and institutional affiliations.



**Copyright:** © 2022 by the authors. Licensee MDPI, Basel, Switzerland. This article is an open access article distributed under the terms and conditions of the Creative Commons Attribution (CC BY) license (<https://creativecommons.org/licenses/by/4.0/>).

## Contents

Abstract.....	1
1. Perspective.....	2
2. Theories of coacervation .....	4
3. Methods used for the determination of coacervates properties.....	8
4. Factors influencing coacervation.....	8
4.1. Ionic strength.....	8
4.2. pH.....	8
4.3. Molecular weight.....	10
4.4. Chirality of the polyelectrolytes .....	10
4.5. Charge density.....	11
4.6. Temperature.....	12
4.7. Solvent.....	13
5. Coacervate Types, Preparation and Properties.....	14
5.1. Simple coacervates.....	14
5.2. Complex coacervates.....	17
5.2.1. Polyelectrolyte-polyelectrolyte.....	17
5.2.2. Polyelectrolyte-surfactant.....	20
5.2.3. Surfactant-surfactant.....	24
5.2.4. Peptide/protein.....	24
6. Applications of Coacervates.....	26
6.1. Wastewater treatment .....	26
6.2. Protein purification.....	28

6.3. Food formulation.....	28
6.4. Cellular mimics.....	29
6.5. Nanoparticle synthesis.....	29
6.6. Delivery carrier.....	30
7. Summary.....	32
References.....	33

## 1. Perspective

Coacervation is a phenomenon in which a colloidal solution gets separated into colloid-rich and colloid-poor phases. The viscous colloid-rich phase is the coacervate which generally stays at the bottom. The upper colloid-poor phase is a dilute equilibrium phase. Generally, two types of “coacervation” are talked about, the simple or self and complex coacervation. In simple coacervation, one type of polymer or surfactant is used in a solvent. The addition of salt, alcohol or a change in pH or temperature results in the separation of phases. In the case of complex coacervation, two oppositely charged polyelectrolytes interact with each other [1]. In this case, also pH, ionic strength, charge ratio, molecular weight, charge density, and some other characteristics of polymers (polyelectrolytes) are important factors. The formation of coacervates is the outcome of a complex balance of electrostatics, hydrophobics, excluded volume, van der Waals, and other contributions to overall system stability. In simple coacervation, soluble complex formation occurs, and they may be called lyophilic colloids. Gelatin, ethyl cellulose, etc., are good examples of polymeric substances which show simple coacervation. Gum Arabic, chitosan, etc., together show complex coacervation. Coacervating agents in the first case are ethanol, water, etc., whereas in the second case, mixed liquids (solutions) are often used. Two polyelectrolytes of different charges are present in the case of complex coacervation and the electrostatic polyelectrolyte–polyelectrolyte interaction leads to an almost neutral charge, i.e., zero, and coacervates start to form. However, it should be noted that quite often, entropic factors are more important than electrostatic interaction in complex coacervation [1,2]. It can be comprehensively stated that simple coacervation involves species such as polyelectrolytes, proteins, peptides, surfactants, and additives such as salts, alcohols, etc. Complex coacervation involves polyelectrolytes, proteins, and surfactants of opposite charges with or without additives.

Coacervates are one of the most intriguing systems in colloid chemistry. The term comes from the Latin words “co” (jointly) and “acerv” (a mound). Colloidal molecules which intend to phase-separate from an aqueous medium in the formation of a second aqueous layer are referred to as “Acerv” [3]. Bungenberg de Jong and Kruyt defined in their original 1929 paper that “the coacervate consists of liquid which in a more or less degree has lost its free mobility” [4]. Recently, Prifits and Tirrell proposed that the formation of coacervates involves a network of dense polyanion and polycation chains kept together by fluctuating electrostatic interactions that are neither strong nor fixed [5]. Primarily, coacervation occurs when a colloidal dispersion separates into two immiscible liquid phases in the same solvent media. These two liquid phases are incompatible and immiscible in the same solvent. Their separation from the liquid to the solid phase causes precipitation. This coacervate phase has higher viscosity and concentration than the preliminary solution, and it has a variety of distinctive characteristics. In fact, depending on its density, the coacervate phase can stay as a turbid suspension of amorphous droplets or coalesce into a top or bottom liquid phase.

Bungenberg de Jong [4] pointed out that the phases are in thermodynamic equilibrium, and the particle surface charges are not only of consideration. It is also known that many coacervate systems are not in thermodynamic equilibrium states but are in metastable states [6]. However, the first report on liquid phase–phase separation (coacervation) is said to be that of Tiebackx who studied a system containing cationic gelatin and anionic

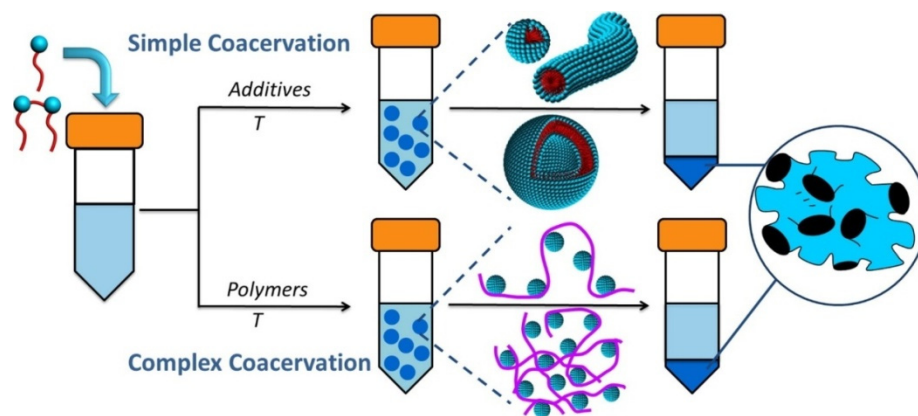
gum Arabic [7]. Turbidimetry, microscopic analysis, light scattering, transmission electron microscopy (TEM), cryogenic transmission electron microscopy (cryo-TEM), scanning electron microscopy (SEM), and cryogenic scanning electron microscopy (cryo-SEM) are crucial methods to study phase separation as well as to characterize the morphology of the coacervate droplets. It has been found that coacervate presents a sponge-like structure, and is also called “sponge phase” or “anomalous phase”. Turbidimetry shows the trend in size change, although not the actual size. It does not distinguish coacervate from precipitate but is useful to study the influence of parameters, such as charge density, ionic strength, pH, and temperature on coacervate phase behavior. Turbidimetry is often paired with optical microscopy for qualitative, phenomenological phase behavior, rather than a quantitative analysis. The coacervate microdroplets are normally polydisperse with a large variation in size and volume, and instability for coalescence. Small-angle scattering techniques, e.g., small-angle X-ray scattering (SAXS) and small-angle neutron scattering (SANS), determine the spatial self-assembling structures with a size of one to several hundreds of nanometers [8].

The “Origin of Life” on earth is an interesting topic which has intrigued human beings for centuries. In general, people used to place this in the realm of religion. However, about a century back, in 1922, a Russian biochemist, Alexander I. Oparin, suggested in a meeting of the Russian Botanical Society that life originated due to the natural laws of the evolution of the universe and the organic compounds were formed by abiogenic synthesis. Around the same time, the British scientist J.B.S. Haldane, independent of Oparin, also suggested a similar idea. Both of them believed that “first life-forms appeared in the warm, primitive ocean and were heterotrophic (obtaining preformed nutrients from the compounds in existence on the early Earth) rather than autotrophic (generating food and nutrients from sunlight or inorganic materials)” [9,10]. They actually believed that “life developed from coacervates, microscopic spontaneously formed spherical aggregates of lipid molecules that are held together by electrostatic forces, and that may have been precursors of cells”. Oparin suggested that coacervates, which are tiny droplets containing high quantities of organic compounds, frequently develop on their own in dilute solutions. As a result, he hypothesized that coacervation was the method by which a fluid phase separated in the ‘primordial soup’ [11], a hypothetical condition which existed on earth some four billion years ago. Haldane also articulated a similar idea [12]. However, no mechanism was suggested by which a coacervate can reproduce, and that is a very serious weakness of the Oparin–Haldane theory. In a recent article, Ghosh et al. [13] suggested that there is evidence, both direct and indirect, where it was seen that the coacervates could have facilitated the transition from membrane-free to membrane-based compartmentalization. They also suggested that this could provide a route to bring RNA and peptides together for convolution. There could have been a multitude of routes wherein a transformation from a chemical to a biological world could have been possible.

The coacervation technique is employed as an encapsulating method, especially in the food and personal care product industries. The utilization of coacervation for the encapsulation of tiny molecules, e.g., proteins, RNA, DNA, and other biomaterials for applications ranging from sensing to healthcare has also received much attention. Moreover, coacervate-linked materials have also found uses in various fields of biomedicine, such as tissue culture scaffolds, cartilage mimics, adhesives for moist, biological settings, etc. [14]. Even coacervate complexes found in natural animals such as mussels, sandcastle worms, and tubeworms are fascinating [15,16].

Like other colloidal aggregates, coacervates are in a state of dynamic equilibrium, and changing the solution condition by adding salt or solvent can cause a single-phase formation, i.e., flocculate or precipitate. The solvent remains trapped between the loops of the macromolecules or colloids as they interact in both simple and complex coacervation. This is referred to as solvent occlusion. Compared to the self-aggregation of surfactants or amphiphilic block co-polymers such as micelles, coacervates are more fluid. In the coacervate, molecules are moving freely as there is no site-specific interaction between the

coacervate-forming substances. Precipitation may occur in spite of coacervation if the charge densities of the constituent molecules are adequately high [17]. In Scheme 1, both simple and complex types of coacervation are shown [18]. In this article, we will discuss the nature, types, and properties of coacervates, probable theories of their formation and existence, as well as their multifarious applications in relation to their synthesis, identification, and characterization.



**Scheme 1.** A schematic representation of the process of simple and complex coacervations using surfactants, polymers, etc., at temperature  $T$ . Additives: pH, salt, solvent, etc. Reprinted with permission from the journal *Advances in Colloid and Interface Science*, 2017, 239, 199. Copyright 2017 Elsevier B.V.

## 2. Theories of Coacervation

The concentration and primary properties (solubility, molecular weight, charge density, and hydrophobicity) of each component as well as their solution conditions (temperature, pH, salt, and solvent) determine the formation of coacervates. The phenomenon is an outcome of a complex balance of electrostatics, hydrophobics, excluded volume, van der Waals, and other contributions to overall system stability. The columbic attraction between oppositely charged species generates electrostatic interaction energy, which is frequently accompanied by a considerable entropy gain owing to counter ion release. Alongside this, the release of the condensed counter ions and water molecules in the hydration shell around the noninteracting chains manifests a significant increase in entropy upon complexation which is orders of magnitude greater than the entropic cost of localization, as well as decreased mobility of the colloid chains into the complex domains. The entropy increase might often surpass the change in enthalpy [19]. In molecular binding, coacervation, and micellization, hydrophobic interactions (the escape of poorly ordered water molecules surrounding the hydrophobic portions of the molecules after hydrophobic binding) result in a huge positive entropy gain. The spontaneity of coacervation (like other self-assembly processes) is favored by high positive entropy change or high negative enthalpy change [2,20]. Thus, considering the above energetic contribution to the formation of coacervate, a straightforward interpretation of the experimental findings is difficult. It has also been suggested that “combinatorial entropy” [21] which happens due to the spatial arrangements of monomers and salt ions is also responsible for the entropy increase. Complex coacervation is where PE-PE (polyelectrolyte–polyelectrolyte) interaction results in neutralization at the required pH in aqueous solution. In this condition, PEs desolvate and mix with each other, resulting in a polymer-rich (coacervate) and polymer-depleted phase. The coacervate droplets can grow from nano- to micro- to meso droplets, and then into a polymer-rich coacervate phase [22].

In a recent article, Ghasemi and Larson [23] described the PE-PE interactions as either physics-based or chemistry-based. A proper theory of this interaction is yet to evolve. Some researchers have defined polyelectrolytes based on chain length, flexibility, charge level, etc., i.e., physical identity (physics-based) [24], whereas some others have stressed

local interactions between monomer and salt species, i.e., chemical identity (chemistry-based) [24]. Both approaches provide some insight, but an overall view remains somewhat elusive. Thus, by merging both approaches together, a quantitative understanding might evolve [25].

The equilibrium thermodynamic principle can be used to explain the coacervation process. Various parameters, e.g., pH, ionic strength of the medium, charge density, etc., affect the process. Interpolymer complexes may lead to the formation of coacervates. Electrostatic forces are important in this interaction, but they are not always dominant. The entropy gain for counterion release can overcome the enthalpic contribution.

It is known that ionic polymers, polyelectrolytes, ionic surfactants, proteins, and biopolymers mostly form coacervates by their mutual interactions. The coacervates may be neutral and ionic also. If we consider two nonionic polymers A and B interact forming a noncovalent complex AB, we may write Equation (1) with the equilibrium constant K shown below with the required activities of the components.



where  $K = a_{AB}/a_A \cdot a_B$

The related standard free energy change is represented in Equation (2)

$$\Delta G^0 = -RT \ln K \quad (2)$$

$\Delta G^0$  is the standard free energy change for the process in Equation (1) at unit activity for both reactants and products.

Two oppositely charged added polyelectrolytes A and B will form the equilibrium,



Here, nS is the number of salt molecules formed from the interaction between the two ionic polymers (polyelectrolytes). For a simple ionic interaction between monoelectrolytes sodium dodecylsulfate (SDS) and cetyltrimethylammonium bromide (CTAB), an ion pair, such as  $CTA^+DS^-$ , and one unit of the salt S (NaBr) are formed in solution. For polymers and polyelectrolytes, more than one molecule of the salt S is formed, hence  $n > 1$ .

Here, like above, the equilibrium constant  $K_s$  is obviously of the form  $K_s = a_{AB} \cdot a_s^n / a_A \cdot a_B$ . It is related to the coacervate-forming process of ionic polyelectrolytes A and B. In comparison with that presented in Equation (1), an extra term  $a_s^n$  arises because of the formation of the salt in the solution. As above,

$$\Delta G_s^0 = -RT \ln K_s \quad (4)$$

Obviously,  $K < K_s$ , and  $\Delta G_s^0 < \Delta G^0$

It may be added that the equations are valid for dilute solutions where activities  $\approx$  concentrations. The addition of salt from outside shall affect K less than  $K_s$ . In the latter, activities shall be affected by the added salts which in the former ought to be negligible as all the species are neutral.

Such a treatment to form a noncovalent complex between A and B in the absence and presence of a ligand L has been presented in the past by Record et al. [26]. The authors also carried out thermodynamic analysis of more complicated systems therein, and interested readers may consult the reference.

It may be added that Kayitmazer [2] followed the rationale of Record et al. considering the salt, S, formed in the reaction (Equation (3)) as a ligand proposed by Record et al. [26] in the equation below.



Here, the ligand L has been considered to have the ability to bind with all the components A, B, and AB. In addition,

$$-\Delta n_L = n_{L,A} + n_{L,B} - n_{L,AB} \quad (6)$$

The equation used by Kayitmazer is:



Interestingly, in both equations, one of the two products has been considered as the ligand. Normally, a ligand is an independent component that undergoes chemical or physicochemical interaction with other components of the system, but herein, it is one of the generated components of the reaction, i.e., L and S in Equations (5) and (7), respectively.

Record et al. also considered Equation (1) as an apparent macromolecular reaction,



where  $K_{app} = a_{AB}/a_A \cdot a_B$ , and  $\Delta G_{app}^0 = -RT \ln K_{app}$

Mixing it with Equation (5) obtained

$$\ln K_{app} = \ln K_T - \Delta n_L \ln a_L \quad (9)$$

Therefore,

$$\Delta G_{app}^0 = \Delta G_T^0 + \Delta n_L RT \ln a_L \quad (10)$$

Several basic steps in obtaining the Equations (9) and (10) are not presented. Interested readers may consult the above-mentioned papers.

From this linear relation 10, we can estimate the slope, i.e.,  $\Delta n_L$ , which is the resultant number of ligand L that contributes to the concerned thermodynamic process we have herein dealt with.

In recent years, thermodynamic studies of micellization and coacervation processes employing the isothermal titration calorimetry (ITC) method have received prominence. In the complex coacervation Section 5.2, we herein present ITC data on some specific systems (cf. Section 5.2.1). We have also studied in the past the thermodynamics of micelle formation of long-chain cationic and anionic surfactants (CTAB and SDS, etc.), and other assembled micellar species, i.e., coacervates, using the ITC method [27].

It may, thus, be stated that the field of coacervates is well open for more basic thermodynamic studies and data analyses.

With the advancement of experimental findings and promising interpretation, several theories on the formation of coacervates have been proposed. The Voorn–Overbeek theory [28] considered coacervation as a battle between electrostatic forces that tend to aggregate charged macromolecules, and entropy factors that tend to disperse them. The Voorn–Overbeek paper and the subsequent Voorn paper [29] deal with complex coacervation on the basis of the “liquid lattice model”, and the Flory–Huggins theory of the thermodynamics of polymer mixing [30]. The well-known Flory–Huggins theory deals with linear-chain polymers in solution. However, it is a fact that although the Voorn–Overbeek theory is being used quite often, it cannot explain the electrostatic contribution to the free energy density for complex coacervates in any concentration regime [31]. They considered short-ranged interactions inside the coacervate using the Flory–Huggins lattice theory [28,32]. Overbeek and Voorn assumed that only Flory–Huggins’s entropy of mixing and electrostatic interactions were important. The rest of the possible interactions were disregarded. The other important assumption was that the charges along the chain backbones are distributed in the phases, and obey the Debye–Huckel theory of monovalent backbone charges, monovalent counter ions, and the salt.

$$G_{\text{elect}} = e^2 / 3\epsilon \left( 4\pi e^2 Nz / \epsilon kTV \right)^{1/2} Nz \quad (11)$$

where  $Nz = \left| \sum n_i z_i \right|$ ;  $V$  is volume of the solution and other symbols have their usual significance. They further obtained

$$G_{\text{elect}}/NkT = -a \left| \sum \sigma_i \phi_i \right|^{3/2} \quad (12)$$

where 'a' is a constant;  $\sigma_i$  and  $\phi_i$  are the charge density of each segment of component  $I$  and volume fraction of each component  $i$ , respectively. By the addition of this quantity to that of Flory–Huggins' results, they obtained a free energy change quantity. They further modified the equations so that the computed results could be experimentally verified. However, there was an anomaly between the experimental and computed results. The details of the calculation can be obtained from the original reference and references therein [1].

Afterwards, Veis [33] modified the former theory considering that the electrostatic interaction is different from that of Voorn–Overbeek. They proposed spontaneous aggregation by electrostatic interaction to form neutral aggregates of low configurational entropy through ion-pair interaction, i.e., the coacervates. The Voorn–Overbeek theory was further extended by Nakajima and Sato [34,35]. They considered charges of the colloids uniformly distributed between the diluted and concentrated phases, including the Huggins interaction parameter in the understanding of the formation of coacervates. The Tainaka theory, originating from the Veis theory, is more general among others, and can be applied to systems with both high and low charge density [36]. According to this concept, coacervation is caused by the attractive forces between the aggregates that grow with the molecular weight and charge density of the polyelectrolytes. All of these early models anticipate coacervation restriction at high ionic strengths, but none of them predict coacervation restriction at low ionic strength. According to a theory proposed for weak polyelectrolytes by Biesheuvel and Stuart [37], coacervation strengthens when the difference between the pK values of the polyacid and polybasic groups is reduced. In this model, they assumed cylindrical cells around every polyelectrolyte chain in the complex and estimated the electrostatic free energy as a function of the complex density using the Poisson–Boltzmann equation. Later, the equilibrium complex density was determined by Flory–Huggins's mixing free energy terms, for certain binary ratios of polycations and polyanions in the associated complex. However, according to Zhang and Shklovskii [38], non stoichiometric coacervation can also be formed by "inter-complex or intra-complex disproportionation".

The random phase approximation (RPA) was used to explain the properties of concentrated systems of weakly charged polyelectrolytes [39] as well as for complex coacervation [6,40]. The formation of small aggregates by ionpairing or some other type of electrostatic correlation has also been considered [41,42]. Sing [6] discussed various present-day theories of complex coacervation with their merits and pitfalls. Some of these are mentioned above. The coacervate systems are charged and highly correlated. They can be described by liquid-state integral equation theories. The connectivity in polymeric systems can be through an extension known as the polymer reference interaction site model (PRISM) which takes care also of the excluded volume effects. The use of this model introduces connected correlations where each monomer along the chain 'observes' neighbors as bonded in the same fashion. PRISM requires a homogeneous, isotropic system. The Voorn–Overbeek model discussed earlier does not consider both connectivity and excluded volume. PRISM allows us to predict measurable quantities such as salt partitioning, and chain connectivity's effects on coacervate phase behavior. It may be mentioned here that the PRISM model needs an iterative solution of (i) the version of the Ornstein–Zernicke equation, and (ii) the Debye–Hückel extended mean spherical approximation. Details of the theory and its use can be found in the reference [43].

The above-discussed models and concepts have both strong and weak points. PRISM describes both Voorn and Overbeek as well as counterion release results at all charge densities. Both local charge organization and phase behavior explained through the assumptions used in the deduction are opaque. Only equilibrium systems are explained, but not quantitatively enough. The RPA theory is useful for equilibrium systems only. In RPA, chain connectivity in polymers is explicitly treated, and, thereby, there is direct unambiguous input of the charge pattern along the chain sequence. RPA treats polymers as Gaussian chains without excluded volumes. Different charge patterns distribute their interactions over the Gaussian-chain conformations differently. Hence, the sequence dependency considered here is absent in the Flory–Huggins (FH) or Voorn–Overbeek (VO) theories. If polymer length is taken as one, RPA results in the Debye–Hückel theory. Furthermore, RPA alone does not explain many observations, whereas an “RPA + FH” model is much better suited to explain experimental observations [44]. Like the VO model, its analytical equations are simple and easy to use. Various ionic charges can be considered with this equation. Highly charged, dense polymers are beyond the scope. Surface tension, free energy, coacervation phase diagrams, etc., can be predicted.

The three foundational problem-solving models, e.g., (i) polymer field theory, (ii) scaling theory, and (iii) counterion release theory, regarding the nature of coacervates have been discussed recently by Sing et al. [45]. The limitation of, as well as relation between, the models is not very clear. It can be noted that the length scale that is observed from RPA is on par with those obtained from the scaling theory [46,47].

### 3. Methods Used for the Determination of Coacervates Properties

Several methods are commonly used to study the phase behavior of coacervates, although the primary means is turbidity that captures the scattering of light by the small coacervate droplets [48–51]. Other methods, such as ionic conductivity [24,52,53], UV-vis [53–55] or fluorescence spectroscopy [56–58], thermogravimetric analysis, [24,59] NMR spectroscopy [52], radiolabeling [60], and quartz crystal microbalance [61], have been used to measure the concentrations of polymers and/or salts therein. Atomic force microscopy [62,63] and surface force apparatus [15,64] have been used to measure the surface properties such as the interfacial tension between the surfactant solution and the coacervate phase. The structural integrity and dynamics of bulk coacervates have also been characterized using rheology [54,61,65–67] along with X-ray and neutron scattering [68–70]. The isothermal titration calorimetry (ITC) method has been used for the determination of the thermodynamics of the formation of coacervates [5–7,35,37,38].

### 4. Factors Influencing Coacervation

The coacervation and the properties of coacervates may be influenced by various environmental conditions such as (i) ionic strength, (ii) pH, (iii) molecular weight, (iv) chirality of the polyelectrolytes, (v) charge density, (vi) temperature, and (vii) solvent, among others. Here, below, we discuss these conditions with examples.

#### 4.1. Ionic Strength

The formation of coacervates is strongly influenced by ionic strength (i.e., the salt concentration in the system). Chollakup et al. [49] employed a PAA/PAH (poly(acrylic acid)/poly(allylamine)) system to investigate the influence of ionic strength on coacervation. Ternary phase diagrams of the PAA/PAH coacervate system's three concentrations of NaCl are shown in Figure 1. It is obvious that at 100 mM NaCl, no coacervate formation is observed at low PAA and PAH concentrations, and at higher concentration, precipitation occurs. At 400 mM NaCl, a limited precipitation region as well as coacervate region is observed. At 1500 mM NaCl, coacervation is observed without precipitation. However, in all cases, solution formation is present. The interaction between opposite-charged col-

loidal particles is basically an electrostatic one that is sensitive to salt screening. The influence of ionic strength on coacervation has been widely explored for different coacervates forming pairs. As per different studies, increased salt concentrations, i.e., ionic strength might prevent the formation of complex coacervates and even help to dissolve them. The screening effect of the additional salt between the charge groups of the opposite-charged polyelectrolytes might explain salt's impact on complex coacervation. The charge-screening effect is known to cause a decrease in Debye length, and a decrease in the capacity of interaction of oppositely charged polyelectrolytes. Increasing the ionic strength decreases the electrostatic interaction between the polycation and polyanion.

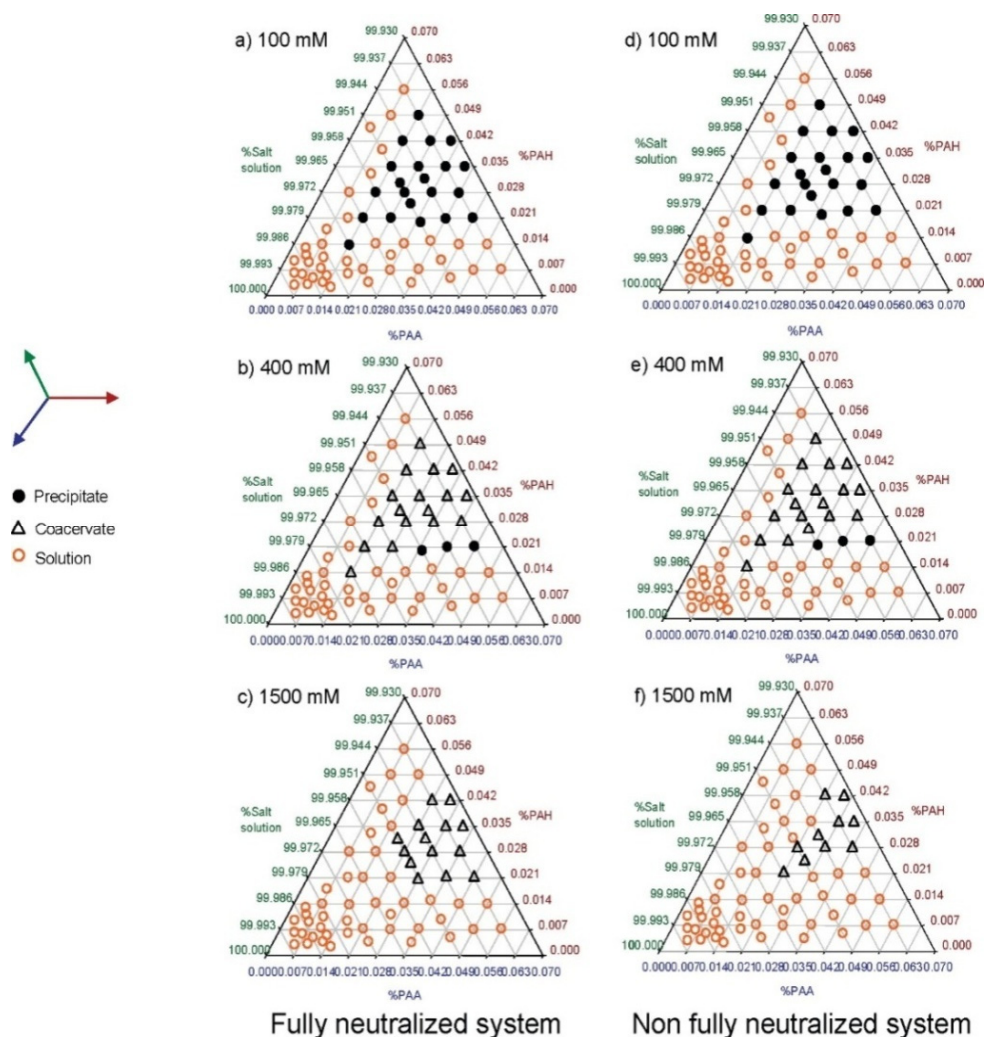


**Figure 1.** Ternary phase diagrams of PAA/PAH mixtures (0.05 wt% total polymer concentration) in aqueous NaCl salt solution (100, 400, and 1500 mM); fully neutralized system: PAANa solution of pH = 8.6 employed (a–c); partially (not fully) neutralized system: PAA solution of pH = 7 employed (d–f). Reprinted with permission from *Macromolecules*, 2010, 43, 2518. Copyright 2010 American Chemical Society.

The influence of ionic strength on the complex coacervation of poly(L-histidine)/poly(L-glutamic acid) (PHis/PGlu) with varied polymer concentration ratios was demonstrated by measuring turbidity as a function of the salt concentration. The authors [45] inferred from the turbidity findings that the presence of a modest quantity of salt in the polyelectrolyte system allows for chain rearrangement, and the creation of bigger coacervate droplets. Beyond 100 mM salt concentration, the gradual dissociation of the polyelectrolyte complex increases due to the screening action of salt on polyelectrolyte charges.

#### 4.2. pH

Joshi et al. [71] studied a mixture of gelatin A and pectin as a function of solution pH 3–9. Light scattering, turbidity titration, and zeta potential studies were carried out. They observed three signature pH transitions, and changes in solution turbidity. The effect of ionic strength ( $I = 0\text{--}0.1$  M NaCl) on the complex formation for various gelatin A–pectin ratios was studied. “It was found that at  $\text{pH} < I_p$  ( $\approx 9$ ), GA electrostatic interactions were dominant while above  $I_p$  such interactions were absent. However, addition of salt led to surface patch binding (SPB) at higher pH, and concentration of GA”.

Kayitmazer et al. [72] studied a mixture of hyaluronic acid (HA) and chitosan (CH), where a variety of phases was observed. It was observed “that the state of the dense phase depends on the molar ratio of HA carboxyl to CH amines and is strongly dependent on their respective degrees of ionization. Due to the strong charge complementarities between HA and CH, electrostatic self-assembly takes place at very acidic pH, but is almost unobservable at ionic strength ( $I$ )  $\geq 1.5$  M NaCl. An increase in either polymer chain length or charge density enhances phase separation.” Polyelectrolytes can have both rod-like and Gaussian coil/ideal chain configurations. The first one happens when monomers are charged with added salt or high (low) pH for the polyacid (bases). The second one happens when the added salt neutralizes the system making low (high) pH for the polyacid (bases).

#### 4.3. Molecular Weight

The polyelectrolyte molecular weight (i.e., chain length) is also an important factor in the coacervation process. Chollakup et al. [73] have also studied the above-mentioned PAA/PAH system as a function of varying PAA molecular weight. They observed that the salt-free systems always gave polyelectrolyte complex precipitates. However, there is a critical salt concentration over which coacervation occurs, and the lower the PAA molecular weight, the lower the critical salt concentration for both precipitate/coacervate and coacervate/solution transitions. Priftis et al. [74] studied a mixture of two polypeptides poly (D,L-glutamic acid Na salt) and poly(D,L- aspartic acid Na salt) by ITC, turbidimetry, and optical microscopy. Complex coacervation was seen when the total polymer concentration was high or the chain length of polypeptides was high. They also studied a mixed system comprising poly (L-ornithin hydrobromide) and poly (D,L glutamic acid Na salt). All probed systems were found to be endothermic. When the salt concentration was increased, the polyelectrolyte charges were affected, resulting in a reduction in the observed energy change and coacervate quantity. The pH played a crucial role in complex formation. Priftis et al. [5] also studied poly(L-Lysine)/poly (Glutamic acid) and established a phase diagram. They, too, observed that the presence of critical salt concentration, and the coacervate composition became a function of the stoichiometry of the mixed polyelectrolytes. In general, the solution turbidity is sensitive to the amount of coacervate during the process of coacervation.

#### 4.4. Chirality

The chirality of polyelectrolytes can also have a significant impact on their ability to form complexes. Perry et al. [75] demonstrated that polyelectrolyte complexes are functions of their chirality when oppositely charged polyelectrolytes are mixed together in solution. Both the electrostatic and hydrogen-bonding interactions are involved in complex formation. Homochiral poly(lysine) and poly (glutamic acid) form solid complexes for any combination of D and L polyanion and polycation. However, liquid coacervates are found when at least one of the polypeptides is racemic, e.g., random copolymer of D and L monomers. Varying amounts of NaCl solutions were used. Visual or optical microscopic characterization was carried out (Figure 2). A delicate balance of forces yields liquid or solid complexes. The process is cooperative in nature. As mentioned above, charge

screening by salt controls the interaction strength. Salt and urea affect the stability of complexes. Chirality determines the physical state of the complexes but also the strength of intermolecular interactions. With an increase in urea concentration, a transition from solid precipitate to liquid coacervate is observed in a mixture of poly (L-lysine) and poly (L-glutamic acid) [75]. As mentioned above, a strong electrostatic interaction between the components, viz., cationic and anionic polyelectrolytes, may lead to precipitation rather than coacervate formation. The presence of salt can control the precipitation phenomenon. The boundary between the precipitate and coacervate is rather broad and the polymer relaxation occurs over this broad region, consuming a reasonably large amount of time. The further addition of salt also has an effect. Time–temperature superposition as well as time–temperature–salt superposition has been observed. In the latter, salt concentration dominates both the precipitation and coacervation [76].

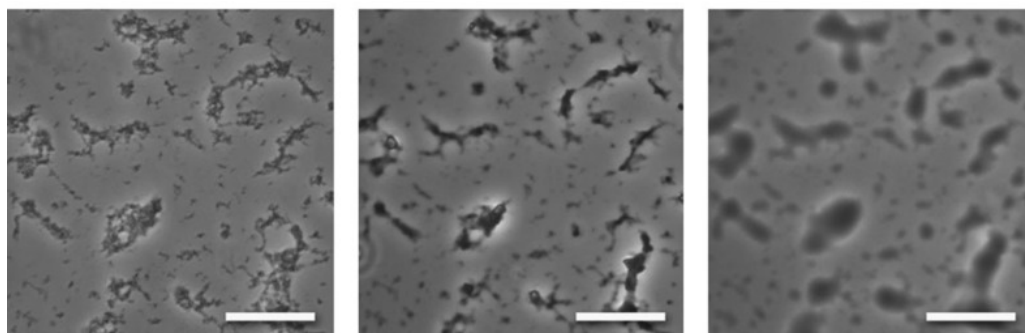


**Figure 2.** Optical micrographs showing the transition from solid precipitate to liquid coacervate for poly (L-lysine) and poly (L-glutamic acid) complexes with increasing urea concentration. Scale bars, 25  $\mu$ m. Reprinted from *Nature Communication*, 2015, 6, 6052. Copyright 2015 Nature Publishing Group.

Kuroyanagi et al. [77] studied how the stereoregularity of polypeptides influences phase behavior for both homochiral and racemic poly(ornithine-co-citrulline) (POC). The separation temperature ( $T_p$ ) for  $\alpha$ -helical polypeptide is higher than the coiled-coil racemic form. Therefore, differences in the secondary structure affect  $T_p$ . The racemic POC form coacervates at  $T_p$ , and  $\alpha$ -helical homochiral POC assembles into a hexagonally packed structure, and precipitates.

#### 4.5. Charge Density

The total charge on the colloid backbone plays a significant role in the formation of coacervate with the opposite-charged colloid. It has been observed from complexation experiments with oligonucleotides and cationic polymers of various chain length, concentration, and structures that liquid coacervates are formed by single-stranded oligonucleotides, whereas solid precipitate is given by double-stranded nucleic acids [78]. The formation of liquids is probably due to low charge density. The addition of salt melts the precipitates into coacervates. In Figure 3, coacervates as well as the irregular solid precipitates are visible. It can be noted here that the charge density of double-stranded DNA is 2.4 times more than the single-stranded one; it is more hydrophilic, less flexible, and has a definite helical structure which leads to specific binding with cations. Charge density has been suggested to be the primary reason for complex phase formation. Kayitmazer et al. [72] also reported a charge-complementary-based coacervate of HA and CH on various mixing orders (see pH section).

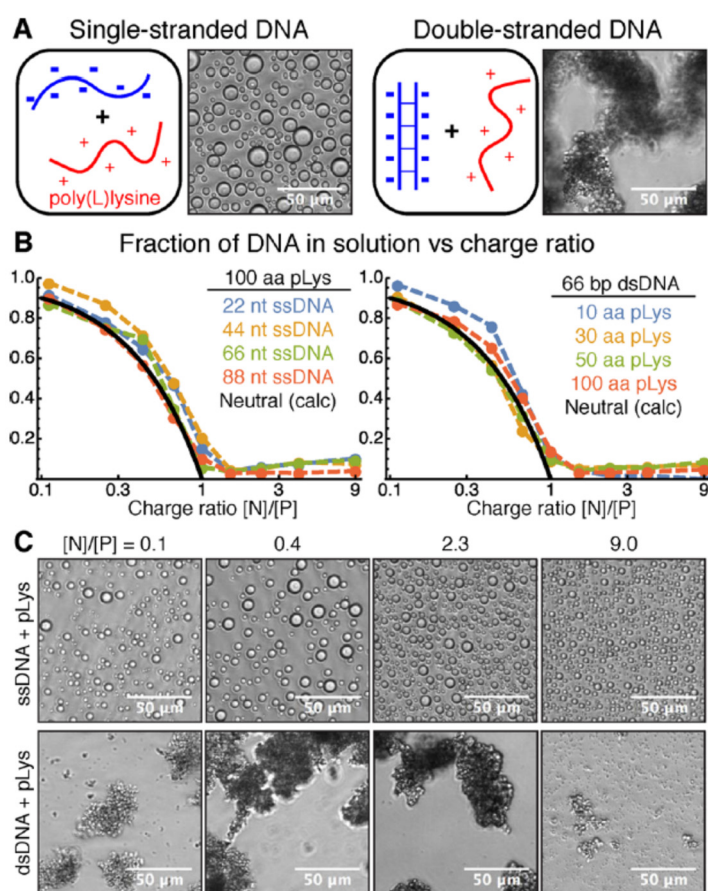


**Figure 3.** Typical micrographs of complexes formed by 22 nt oligonucleotides and 50 amino acid pLys peptides mixed at equal charge (amine and phosphate) concentration. Reprinted with permission from *JACS*, 2018, 140, 1632. Copyright 2018 American Chemical Society.

A series of experiments were carried out by Cummins and Obermeyer [79] with cationic supercharged green fluorescent protein (GFP) and oppositely charged polyanionic macromolecules. They studied the phase behavior of the mixed system. Phase separation was observed at various mixing ratios, salt concentrations, and pHs. Proteins with higher charge density phase-separated over a broader pH and salt range in comparison to proteins with lower charge density. Liquid/liquid phase separation was observed for most systems by optical microscopy. However, the GFP/DNA system formed solid aggregates.

Furthermore, Aumiller Jr. and Keating [80] studied phosphorylation-mediated RNA/peptide complex coacervation. They observed electrostatic interactions between the short cationic peptides as well as the longer polyanionic RNAs. This interaction is responsible for phase separation. Coacervates were also formed on silica beads. The total charge on the colloid backbone plays a significant role in the formation of coacervate with an opposite-charge colloid. It is also obvious from the above discussion that temperature, concentration, solvent, etc., have tremendous influence on the coacervation process.

#### 4.6. Temperature

The temperature can influence the coacervation process through a number of pathways. Both the interplay between enhanced hydrophobic interactions and increased polyelectrolyte dissociation are closely related to the changes in temperature. The effect on the formation of coacervation can be attributed to the changing degree of ionization with temperature. The interaction between polyelectrolytes decreases with increasing temperature since the coacervation is electrostatic. Anvari et al. [81] investigated the rheological and structural characteristics of fish gelatin (FG)–gum Arabic (GA) complex coacervate phase

as a function of phase separation temperature. This coacervate was obtained from an aqueous mixture of 1% FG and 1% GA at pH 3.5. As the phase separation temperature changed from 40 to 10 °C, they observed a viscous coacervate phase formation which had a larger volume fraction and higher biopolymer concentrations. It showed a more condensed microstructure with a solid-like elastic behavior in the phase separated at 10 °C. A rigid and thermostable coacervate gel and an increase in the gelling and melting temperatures of the coacervate phase (3.7–3.9 °C and 6.2–6.9 °C, respectively) were seen. The coacervate gel was a weak physical gel reinforced by FG–GA attractive electrostatic interactions.

Ali et al. [55] demonstrated phase separation upon heating mixtures of polyelectrolytes potassium–poly(styrenesulfonate) (KPSS) and poly(diallyl dimethylammonium bromide) (PDADMAB) with added KBr. The presence of lower critical solution temperature (LCST) was observed. With increasing KBr concentration, the LCST coexistence curves became narrow and reduced the polymer concentration ( $C_p$ ) in the polymer-rich phase. Positively charged protamine (Mol.wt ~4 kDa) and multivalent anions (citrate, triphosphate, mol. Wt. < 0.4 kDa) showed complex coacervation. The system had an upper critical solution temperature (UCST) and was reversible with temperature cycling. Generally, however, complex coacervates with two oppositely charged polyelectrolytes showed lower critical solution temperature (LCST). It formed a dense liquid phase with dilute supernatant outside. No gel formation was observed, probably because the electrostatic force was not strong enough. The enthalpic-origin phase transition showed UCST behavior [82]. Nakashima et al. [83] discussed a minimal, nucleotide-based coacervate model for active droplets. According to them, the coacervate droplets form, and do not undergo Ostwald ripening, and the droplet growth rate reflects experimental conditions such as substrate, enzyme, and protein concentration. For details, their publication may be consulted [83]. A molecular dynamics simulation study of a protein (lysozyme)- polyelectrolyte (poly(styrene sulfonate) or polyphosphate) complex was carried out. The proteins were of different degrees of polymerization. The short, charged chains are mostly bound to the proteins through repeat units whereas long chains, which have higher charge, do have unbound fragments. They form charged loops and tails around the protein surface. These loops are said to provide stability to the complex [84].

#### 4.7. Solvent

The complexation of polyelectrolytes is inhibited by the presence of organic solvent due to the weakening interactions between the polycation and polyanion in a low-dielectric-constant environment. Meng et al. [85] prepared a complex coacervate by mixing Poly[(vinylbenzyl) trimethylammonium chloride] (PVBTMA) and poly(sodium 4-styrenesulfonate) (PSS) polyelectrolytes in the presence of NaBr in the aquo-organic (ethylene glycol–water or ethanol–water) mixed solvent medium. As PVBTMA and PSS have a strong interaction between them, they get precipitated in an aqueous medium, but in the presence of salt and aquo-organic medium, they form coacervate. This could only happen due to the weakening of the strong electrostatic interaction with the decreasing polarity of the solvent. Danielsen et al. [86] also demonstrated the complex coacervation of cationic conjugated polyelectrolyte poly(3-[6'-{N-butylimidazolium}hexyl]thio -phene) bromide and anionic sodium poly(styrenesulfonate) in tetrahydrofuran (THF)–water mixtures. It was observed that the polymer pairs got precipitated at low THF concentration but they formed coacervates at a higher proportion of the THF mixture.

A molecular dynamics simulation was carried out by Khavani et al. [87] to understand various forces and solvation acting on the effect of ethanol solvents on PDADMAc and PSS pairs in aqueous solution.

In addition to the above factors, the molecular topology and branching, hierarchical architecture, etc., of constituting substances also play a significant role in coacervation.

## 5. Coacervate Types, Preparation, and Properties

Coacervations are of two types, simple and complex. The simple process uses solutions of one type of molecules (surfactant, polymer, protein, polyelectrolyte, etc.), and treats them under varied environmental conditions, i.e., pH, temperature, solvent, salts, pressure, etc., to generate coacervate phases useful for varied purposes. They are then characterized by the different methods mentioned above. In the complex process, two different types of polymeric, surface-active compounds of the class mentioned above are mixed to generate complex coacervates which can be also controlled according to choice by altering the environmental conditions stated above. The second type is more versatile and useful, and is cultivated much more than the first type, i.e., simple coacervate. A simple documentation of both types of coacervates and their formation conditions are presented in Table 1 below.

**Table 1.** An appraisal list of some simple and complex coacervate-forming systems.

Simple Coacervation		Complex Coacervation		
Polymer	Coacervating agent	Polymer 1	Polymer 2	Coacervating agent
Bovine Serum albumin	Ethanol	Gum Arabic	Gelatin	
Chitosan	NaOH	Gum Arabic	Chitosan	
Ethyl Cellulose	Water	Chitosan	Gelatin	
Gelatin	Acetone	Poly(lactide)	Poly(lactide-co-glycolide)	Silicone oil
Gelatin	Acetone + ethanol	Chitosan	Hyaluronic acid	Na-acetate
Soy glycinin	Acidic water	Hydroxyethyl-cellulose	Sodiumsarcosinate	Isopropanol-water

### 5.1. Simple Coacervates

The presence of a dehydrating agent (either solvent or salt or both) might cause simple coacervation by favoring colloid–colloid interactions over colloid–solvent interactions. Conventional surfactants, such as monomeric surfactants, are the most extensively used. When the concentration of monomeric surfactant molecules exceeds their critical micelle concentration, they tend to aggregate into micelles. In aqueous solution, these micelles are homodispersed and stabilized by their surface charges and hydration shell. At room temperature, a single monomeric surfactant cannot generally self-assemble into coacervates. However, a single-chain surfactant also turns to a coacervate phase at an elevated temperature and/or in the presence of salt or solvent in the solution.

Zhou et al. [88] used turbidity titrations, cryo-TEM, and light microscopy to investigate coacervates based on the spontaneous phase separation of a single-chain surfactant (–) -*N*-dodecyl-*N*-methylephedrinium bromide (DMEB) in the presence of NaCl, CaCl<sub>2</sub>, and MgCl<sub>2</sub>. They are easily produced at low DMEB concentration and stay stable throughout a wide pH range 2–10. A variety of dyes (methylene blue, rhodamine 6G, calcein, fluorescein, and Nile red) and biomacromolecules (DNA) are spontaneously taken up and stay functional within the coacervates. The majority of observed coacervations for single gemini surfactants occurred in a sequence of zwitterionic gemini surfactants with varying alkyl chain lengths. Two simple amphiphilic moieties are connected by a spacer group amid the head group in gemini surfactants. Menger et al. [89] revealed that a zwitterionic gemini surfactant may build a sponge-like architecture and aggregate into coacervates of 1 to 5 wt%. They came to the conclusion that the electrostatic association of counterions with surfactants changes spontaneous aggregates to coacervate. Gemini surfactants, unlike standard single-chain surfactants, are more likely to create coacervation without the

need for additives. Huang et al. [90] found that a pH-sensitive carboxylic gemini surfactant, 4,8-dioctyl-3,9-dioxo-6-hydroxy-4,8-diaza-1,11-undecanedicarboxylate (SDUC), produces an oily phase (coacervate) in aqueous solutions at a pH of  $\sim 4.1$ , but at a higher pH, it forms vesicles. The coacervation is caused by inadequate electrostatic repulsion and greater hydrogen bonding among the carboxylic groups of SDUC at lower pH.

Mohanty and Bohidar [91] studied the coacervation of gelatin-B in aqueous alkaline solution by titrating with alcohols (methanol, ethanol, propanol, and tert-butyl alcohol) in the pH range of 5–8 and ionic strength of 0.01–0.10 M NaCl. The system obtained turbidity because of the formation of coacervate which maximized, and then precipitate formation was noted. Intermolecular folding, aggregation, and formation of microcoacervate droplets occurred in the system which was monitored by the DLS method. Solute–solvent interaction also led to gelation in the system. Manaf et al. [92] studied the encapsulation of citronella essential oil by simple coacervation of Arabic gum by controlling pH, temperature, oil–gum proportion, starting rate, and time. The efficiency of encapsulation was 94%, and the rate of release of the oil from the coacervate was 0.0617 volume% per hour. They also carried out the same study by complex coacervation in Arabic gum and gelatin. The efficiency of formation was close to the first, but the kinetic rate of release was 1/3 of the first. Figure 4 shows the capsule morphology of simple (left) and complex (right) coacervates.

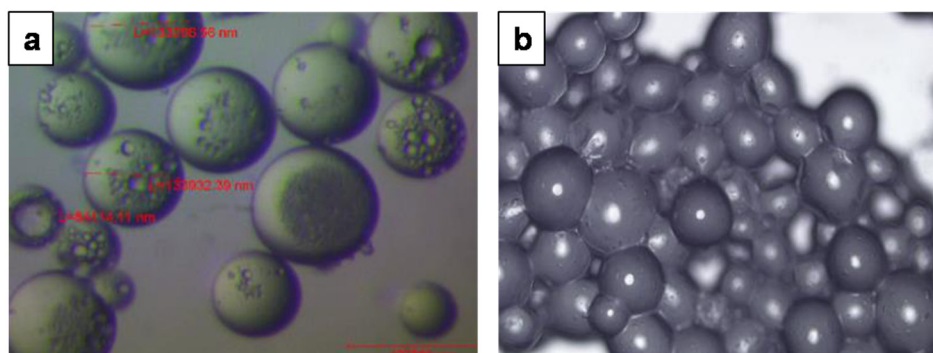


**Figure 4.** Morphology of capsules under a light microscope with a 10 $\times$  magnification objective. (a): Simple coacervation freshly after capsules' harvesting. (b): Complex coacervation freshly after capsules' harvesting. Reprinted from *IOP Conf. Ser. Mater. Sci. Eng.*, 2018, 358, 012072. Copyright 2018 IOP Science.

Perro et al. [93] studied a simple coacervate system which can be used in an encapsulation application. Negatively charged polyacrylic acid polymer chains were partially cationized using diamine and carbodiimide chemistry-affording ampholytes, named PAA-DA, with a tunable charge ratio. At pH 7, PAA-DA was soluble, but near the isoelectric point, a phase separation occurred. Coacervation was seen only for a given amine-to-acid ratio. Above pH 4, coacervates were destroyed, although the presence of calcium ion increased the coacervate stability by inducing gelation in the system.

The coacervate droplets spontaneously sequester entities ranging from small to macromolecules. By changing pH or by removing calcium, triggered release can be obtained. Self-coacervation has been suggested as of interest in pharmacy, water treatment, food science, or diagnostics. Soy glycinin, which behaves as a wall-forming material, was used by Lazko et al. [94] to encapsulate hexadecane. The deposition of coacervated glycinin around hexadecane gets enhanced at pH 2 and 55  $^{\circ}$ C. There was “correlation between glycinin concentration in the continuous phase, specific surface of the dispersed phase and the microencapsulation efficiency”.

Rizvi et al. [95] reported that the thermodynamically stable block copolymer coacervates made from polyethylene oxide block-poly methyl methacrylate (PEO-b-PMMA), poly dimethylacrylamide- block-poly methyl methacrylate (PDMA-b-PMMA), and poly (ethylene oxide)-block-poly (caprolactone) (PEO-b-PCL) individually in mixtures of aquo-

organic solutions (dioxane–water, tetrahydrofuran–water, and acetone–water). The hydrophilic block is soluble, while the hydrophobic block is sparingly soluble in solutions with intermediate water content (water volume fraction,  $\phi_w$  approximately 0.25–0.40). The moderate variation in solubility is not enough to cause block segregation. As a result, the block copolymers form coacervates. Figure 5 depicts an example of PEO<sub>45</sub>-b-PMMA<sub>300</sub> coacervation.

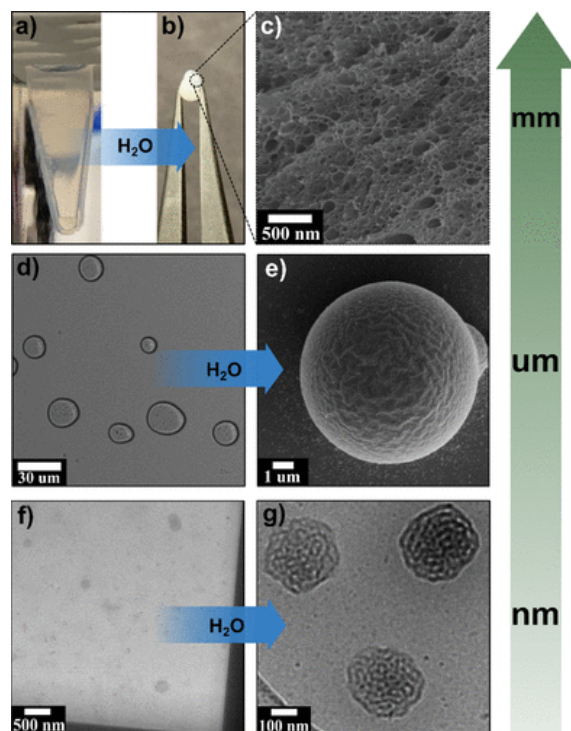


**Figure 5.** Macroscale to nanoscale self-assembly formation of PEO<sub>45</sub>-b-PMMA<sub>300</sub> system. (a) Photograph of a macrophase-separated coacervate solution of PEO<sub>45</sub>-b-PMMA<sub>300</sub> at  $\phi_w = 0.25$  in dioxane. (b) Photograph of a millimeter-size pellet formed by driving the coacervate phase to self-assembly via excess water addition. (c) SEM image of a cross section of the pellet formed showing the bicontinuous microstructure within the self-assembled pellet. (d) Bright-field optical microscopy image of the dispersed coacervate droplets of PEO<sub>45</sub>-b-PMMA<sub>300</sub> at  $\phi_w = 0.25$  in the dioxane mixture. (e) SEM image of the microparticles self-assembled from the dispersed coacervate solution via excess water addition. (f) In situ TEM image of nanocoacervates formed using PEO<sub>45</sub>-b-PMMA<sub>300</sub>. (g) Cryo-TEM image of continuous structures formed at  $\phi_w > 0.3$  water in dioxane on the cryo-TEM grid. Reprinted with permission from *Macromolecules*, 2020, 53, 6078. Copyright 2020 American Chemical Society.

As there are very few self-coacervation studies of plant proteins, the self-coacervation of soy glycinin and its transformation into hollow condensates studied by Chen et al. [96] may be herein cited. Here, the hexameric structure of the protein (composed of hydrophilic and hydrophobic polypeptides) is crucial for the process. In the acidic polypeptides, there is charge screening which allows for weak hydrophobic interactions between exposed hydrophobic polypeptides. They find order in the coacervate surface and that stabilizes the coacervate shape during hollow-condensate formation. Aging enhances the stability of both coacervates and hollow condensates. The authors opined, “Understanding plant protein coacervation holds promises for fabricating novel functional materials” [96].

## 5.2. Complex Coacervates

### 5.2.1. Polyelectrolyte–Polyelectrolyte Types

Oppositely charged polyelectrolytes (PE) are frequently employed in complex coacervation studies. They are characterized as linear macromolecule chains with several

charged groups that are commonly dissociated in water or other polar solvents, resulting in charges throughout the polymer chain. DNA, protein, and polysaccharides are examples of natural PEs. PEs can be negatively charged (polyanion) or positively charged (polycation), depending on the functional groups, such as polyacrylic acid (PAA) and sulfonated polystyrene (PSS), and polyethyleneimine (PEI), poly(*N,N*-dimethylamino-ethyl methacrylate) (PDMAEMA), and poly(diallyldimethylammonium chloride) (PDADMAC). PEs are categorized into two forms. One is a “strong polyelectrolyte”, such as PSS, which is completely dissociated in water and has a practically pH-independent ionization degree. “Weak polyelectrolytes”, such as PAA, are another form of polyelectrolyte whose ionization degree is substantially controlled by solution pH. The formation of a polyelectrolyte complex (PEC) is based on the strong interaction of polycation and polyanion guided by the thermodynamics of the process.

Complex coacervation forms when oppositely charged polyelectrolytes are mixed under certain conditions. Numerous investigations using bio- and synthetic polyelectrolytes have been conducted in this field. Table 2 shows some coacervate systems formed using combinations of polyelectrolytes under some physicochemical conditions.

**Table 2.** The formation of coacervates by representative oppositely charged polyelectrolyte pairs and corresponding formation conditions.

Polyelectrolyte Pairs <sup>a</sup>	Ionic Strength [ $\times 10^{-3}$ M]	pH Range	Reference
PDADMAC/PMAA	0–400	-	[97]
PDADMAC/PSS	1300–1800	-	[52]
PDADMAC/P(E-alt-MA)	-	>6	[98]
PDADMAC/PAA	300–3000	3–9	[99]
PAH/PAA	0–4700	5–9	[49]
PEI/PAA	-	2–7	[100]
PDMAEMA/PAA	50–3000	3–8	[99]
PMAA/PMOETAC	200–500	-	[97]
PEI/PVS	-	2–10	[100]
PAH/P(E-alt-MA)	-	6–9	[98]
PDADMAC/PANa	-	7, 10	[101]
PDADMAC/BSA	100	7.7	[102]
Chitosan/BSA	100	4.0	[102]
PAAD/PGNa	250	9.1	[103]

<sup>a</sup>PDADMAC: Poly(diallyldimethylammonium)chloride, PSS: poly(styrenesulfonate); PDMAEMA: poly(*N,N*-dimethylaminoethyl methacrylate); PAH: Poly (allylamine hydrochloride); PAA: poly(acrylic acid); PEI: polyethyleneimine; PVS: poly(vinylsulfonic acid); P(E-alt-MA): poly(ethylene-alt-maleic acid); PMAA: poly(methacrylic acid, sodium salt); PMOETAC: poly(2-(methacryloyloxyethyl)trimethylammonium chloride); PANa: poly(sodium acrylate); PGNa: poly(sodium L-glutamate); PAAD: poly(amido amine) dendrimer.

Vitorazi et al. [101] reported an interesting thermodynamical observation of PDADMAC and PANa coacervation formed by a two-step process. For thermodynamic analysis, the ITC experimental technique was used to quantitatively study a broad range of self-association and intermolecular interactions. They studied this by adding PDADMAC to PANa (type I) or vice versa (type II) using ITC, light scattering, and electrophoresis methods. Both types of results concur well with one another for all methods.

The primary process begins at low charge ratios and is associated with a sigmoid-like reduction in enthalpy. The secondary process follows emerging a smooth endothermic peak. The ITC data were analyzed and reported using a modified version of the multiple noninteracting sites (MNIS) model that specifies the thermodynamic parameters for each reaction to account for the generated binding isotherms (Figure 6). Throughout the

investigation, small positive enthalpies and significant positive entropies compatible with a counterion release were observed. The obtained data are shown in Table 3.

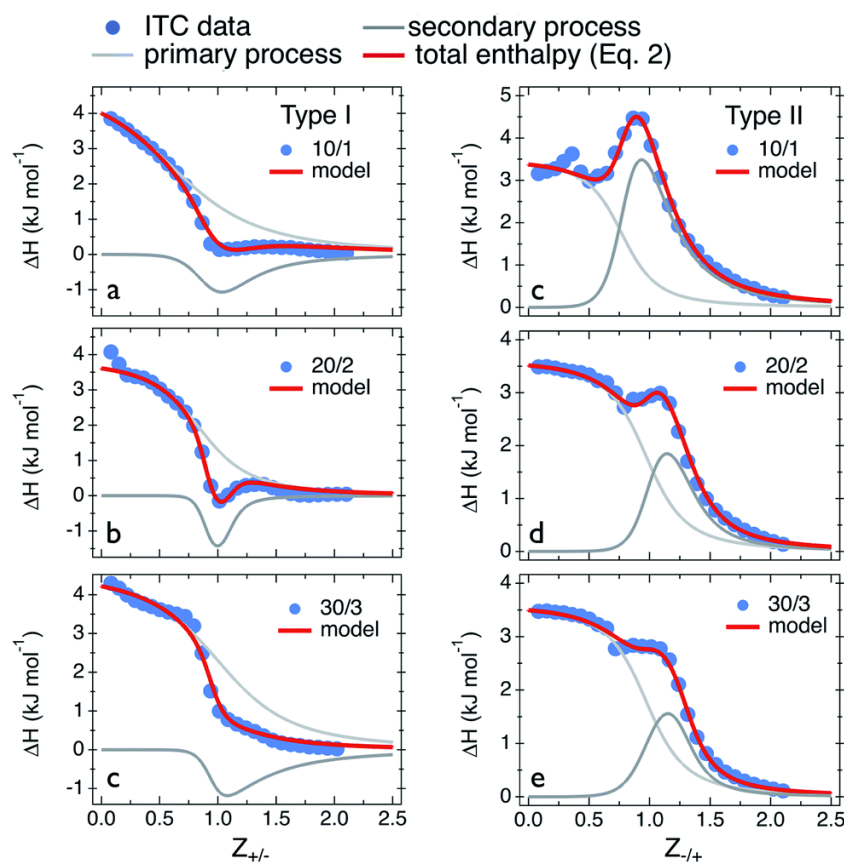


**Figure 6.** ITC-generated binding isotherms of the PDADMAC/PANa system at different concentrations. Type I (left panels) and Type II (right panels). The continuous lines through the data points were obtained through fitting of the MNIS model. Reprinted with permission from *Soft Matter*, 2014, 10, 9496. Copyright 2018 Royal Society of Chemistry.

**Table 3.** Thermodynamic parameters for primary and secondary processes obtained from the adjustment of the ITC curves with MNIS model fitting.  $\Delta H_b^A$ ,  $K_b^A$ ,  $n_A$ ,  $\Delta G^A$ , and  $\Delta S^A$  denote the binding enthalpy, binding constant, stoichiometry, free energy, and entropy changes, respectively. Reproduced with permission from *Soft Matter*, 2014, 10, 9496. Copyright 2018 Royal Society of Chemistry.

Primary Process	$\Delta H_b^A$ (kJ mol <sup>-1</sup> )	$K_b^A$ (M <sup>-1</sup> )	$n_A$	$\Delta G^A$ (kJ mol <sup>-1</sup> )	$\Delta S^A$ (J mol <sup>-1</sup> K <sup>-1</sup> )
Type I: PDADMAC in PANa					
10/1	5.0	$5.0 \times 10^3$	0.8	-21.1	87.5
20/2	3.8	$8.3 \times 10^3$	0.9	-22.4	87.9
30/3	4.6	$3.3 \times 10^3$	1.1	-20.1	82.8
Type II: PANa in PDADMAC					
10/1	3.5	$3.3 \times 10^4$	0.8	-25.8	98.3
20/2	3.4	$1.6 \times 10^4$	1.0	-24.1	92.0
30/3	3.6	$1.1 \times 10^4$	1.0	-23.1	89.5
Secondary Process	$\Delta H_b^C$ (kJ mol <sup>-1</sup> )	$K_b^C$ (M <sup>-1</sup> )	$n_C$	$\Delta G^C$ (kJ mol <sup>-1</sup> )	$\Delta S^C$ (J mol <sup>-1</sup> K <sup>-1</sup> )

Type I: PDADMAC in PANa					
10/1	-2.6	$2.0 \times 10^4$	1.1	-24.5	73.5
20/2	-2.1	$1.0 \times 10^5$	1.1	-28.5	88.6
30/3	-3.0	$3.3 \times 10^3$	1.1	-20.1	57.3
Type II: PANa in PDADMAC					
10/1	7.0	$2.5 \times 10^4$	1.05	-25.1	107.6
20/2	3.9	$3.3 \times 10^4$	1.3	-25.8	99.6
30/3	2.5	$3.3 \times 10^4$	1.3	-25.8	94.9

Leinser and Imae [103] prepared a coacervate using a combination of poly (sodium L-glutamate) (PGNa) and poly (amido amine) dendrimer (PAAD) in the aqueous medium containing 250 mM NaCl at pH 9.1. They explain the formation of coacervate through interpolyelectrolyte complex (IPEC) formation. Colloid aggregation to microgel to coacervate occurred depending on the PGNa/PAAD ratio. The microstructures of the microgel and the coacervate were similar, as was found from SAXS data analysis.

Li et al. [104] reported a comparative study of PDADMAC/PSSNa and PDADMAC/PANa systems, and observed a striking structural difference at the charge ratio  $Z=1$ . They concluded from the DLS, turbidity, electrophoresis, and interfacial surface tension data that the highly electrostatic interacting system PDADMAC/PSSNa went through a liquid–solid phase transition resulting in solid aggregates, whereas the weakly interacting PDADMAC/PANa system went through a liquid–liquid phase transition forming coacervate droplets as illustrated in Figure 7.

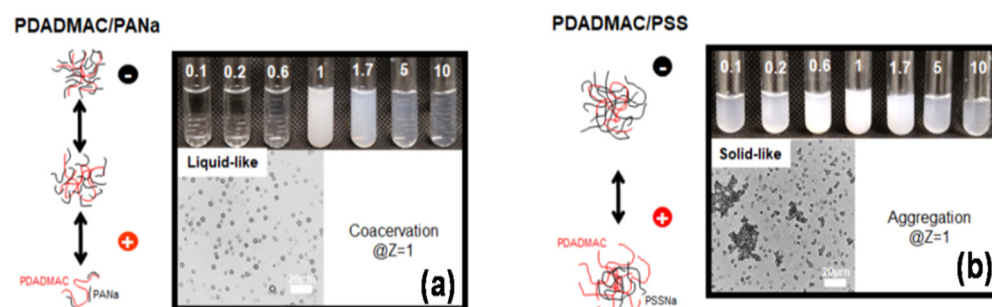


**Figure 7.** Photographs of the PEC dispersions taken at different Z values together with microscopic images taken at charge stoichiometry ( $Z = 1$ ) of PDADMAC/PANa (a) and PDADMAC/PSSNa (b). Reprinted with from *Polymers*, 2021, 13, 3848. Copyright 2021 MDPI.

Yang et al. [105] predicted the co- and counterions' role and their position in the coacervates of poly(diallyldimethylammonium) (PDADMA) and poly(styrene sulfonate) (PSS) systems using ITC and the radio labeling of added salts (Figure 8). Their prediction through two different ways is mentioned in the legend of the figure.

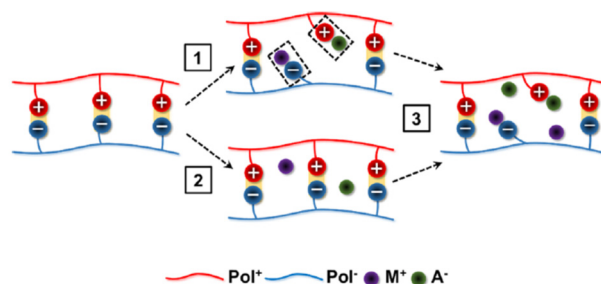


**Figure 8.** An ion-free coacervate is shown on the left. Salt ions  $M^+$  and  $A^-$  dope the coacervate, either by breaking the  $Pol^+Pol^-$  pairs and acting as counterions (path 1) or by not formally breaking the

Pol<sup>+</sup>Pol<sup>-</sup> pairs but remaining as co-ions (path 2). Paths 1 and 2 can occur sequentially or simultaneously to give a mix of counter- and co-ions (shown on the right). Reproduced with permission from *Macromolecules*, 2020, 53, 5465. Copyright 2020 American Chemical Society.

Joy et al. have worked on different coacervates based on biodegradable, thermoresponsive polyester polyelectrolytes, and they have used such coacervates for the encapsulation of different hydrophobic materials [106–109].

### 5.2.2. Polyelectrolyte–Surfactant Types

Water-soluble synthetic and modified polymers, viz., polyethylene oxide, polyethylene glycols, poly(diallyldimethylammonium) chloride (PDADMAC), poly(vinylpyrrolidone) (PVP), carboxy-methyl cellulose (CMC), and their hydrophobically modified products, other carbohydrate polymers (starch, amylose, amylopectin, etc.), and proteins (bovine serum albumin, lysozyme, gelatin, hemoglobin, pepsin, papain, egg albumin, etc.) have ample uses for their interaction with different amphiphiles. These polymeric compounds may be used to produce coacervates choosing appropriate and matching molecular structures, and/or adjusting environmental conditions. Block copolymers and graft copolymers may also be employed in the preparation process.

The Dubin group [110–113] has studied the complicated coacervation of oppositely charged polyelectrolyte/mixed-micelle systems in aqueous medium. A model system comprising strong polycation PDADMAC and oppositely charged mixed micelles of anionic surfactant SDS and nonionic surfactant Triton X-100 (TX100) was used to study complex coacervation. The strong electrostatic interaction of PDADMAC with SDS usually produces precipitation. The charge density of the SDS-TX100 mixed micelles is low enough to make suitable polyelectrolyte/micelle complexes for coacervation by adding nonionic surfactant TX100 and altering the SDS/TX100 molar ratio.

They found three diffusional modes in the single-phase samples and in the coexisting coacervate phases. A cryo-TEM image of the coacervate of PDADMAC/TX100-SDS is shown in Figure 9. In the dilute domains, polymer-bound micelles appear largely as 10 nm dots. The needs of overall charge neutralization, ionpairing, and counterion release during coacervation are thought to be the source of the results found.

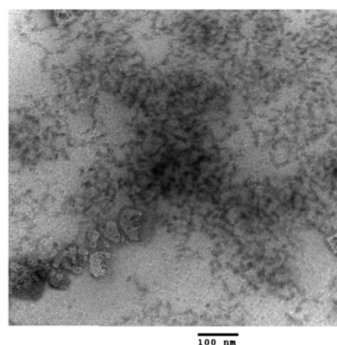
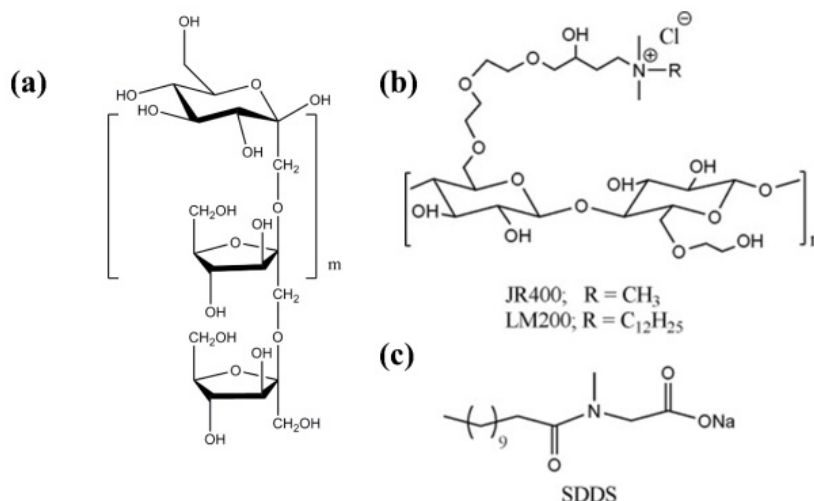


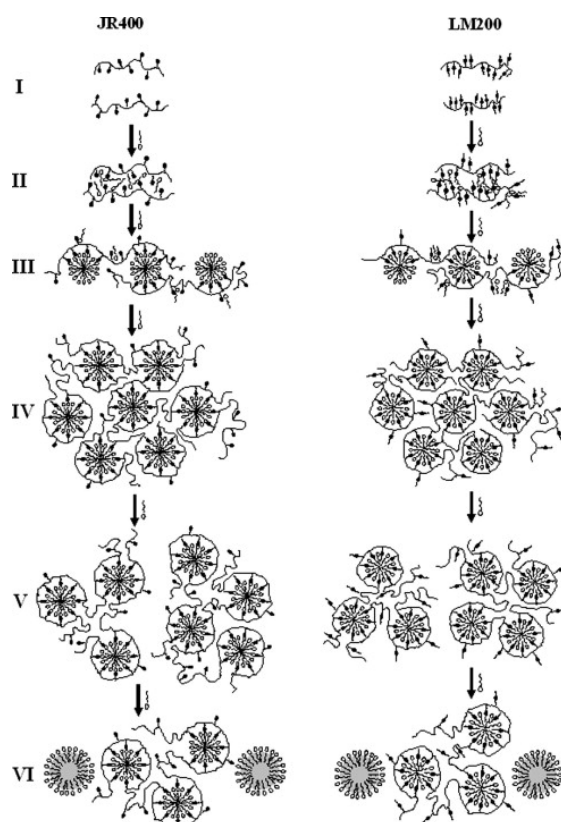
**Figure 9.** Cryo-TEM image of PDADMAC/TX100-SDS coacervate system. Reproduced with permission from *Soft Matter*, 2013, 9, 7320. Copyright 2013 Royal Society of Chemistry.

Our group studied the complexation, aggregation, and coacervation of the amphiphile SDDS (Sodium N-Dodecanoylsarcosinate) with the cationic hydroxyl ethyl celluloses (Scheme 2) [114]. SDDS monomers interacted with the polymers resulting in bound, small-micelle aggregates. At a higher concentration of SDDS, the complexes self-associated, forming turbid coacervate phases. At a further increased SDDS concentration, the coacervates disintegrated. The turbidity decreased by way of the formation of increased normal SDDS micelles. The net charge on the polymer reduced with amphiphile addition, passed through the point of neutrality, and became oppositely charged with ex-

cess addition of SDDS. Depending on the nature of the polymer and the amphiphile, turbid, viscous, and even gel-like consistencies can arise in the solution. The molecular structures of the polymeric hydroxyl celluloses inulin, JR400, LM200, and the surfactant SDDS are presented in Scheme 2. The formation of different complexes and aggregates in solution is illustrated in Scheme 3 [114].



**Scheme 2.** Structures of (a) biopolymer inulin, (b) cationic celluloses JR400 and LM200, and (c) sodium dodecanoylsarcosinate (SDDS).



**Scheme 3.** Different stages of the interaction of JR400 and LM200 with SDDS in an aqueous medium. (I) Individual polymer chains in dilute solution. (II) The appearance of a kind of polymer induced amphiphilic assemblies with the addition of SDDS. (III) Formation of well-defined, normal, small micelles (for JR400) and induced mixed micelles (for LM200) at CAC. (IV) Aggregated assemblies of the polymer-micelle complexes forming coacervates. (V) Disintegration of the coacervates at Cs

$< [SDDS] > CMC_e$ . (VI) Complete disintegration with the formation of a free necklace–bead-type complex and free normal SDDS micelles in solution at  $[SDDS] \gg CMC_e$ . The detailed conductance, surface tension, turbidity, and viscosity of the studied systems were measured to arrive at the conclusion. The terms  $C_s$  and  $CMC_e$  designate the maximum binding state of small aggregates on inulin, and the maximum surfactant to form free micelles in solution, respectively. Reprinted with permission from *J. Phys. Chem. B*, 2009, 113, 8505. Copyright 2009 American Chemical Society.

We have also examined the nature of interactions between the carbohydrate polymer inulin and the cationic amphiphiles, alkyl trimethylammonium bromides ( $C_n$ TAB:  $n = 12, 14, 16,$  and  $18$ ), over a fair range of concentrations of both the polymers and the amphiphiles [115]. Similar results to those presented above were observed. Micellar aggregates, their binding with inulin followed by aggregation yielding turbidity followed by its reduction, and finally the formation of larger amphiphile micelles along with inulin complexes occurred in solution. Tensiometric, conductometric, viscometric, and turbidimetric methods were employed to explore the observed phenomena. The morphology, structure, and thermal stability of the formed complexes (including coacervates) between inulin and  $C_{18}$ TAB were examined using SEM, TEM, AFM, DSC, TG, and DTA methods.

Free inulin A (0.5%  $w/v$ ) is of prolate shape (Figure 10i(A)). In the presence of OTAB  $< C_T$  (B), the coacervates are elongated shapes (Figure 10i(B)); above  $C_T$  (C), the population of large size diminishes (Figure 10i(C)) resulting in the formation of small sizes as explained above. In Figure 10ii(D), the FESEM morphology of inulin assembly appears as aggregated globules. In the presence of  $[OTAB] > C_T$ , randomly assembled, thread-like structures of the complex appear (Figure 10ii(E)). The phenomenon of coacervation is documented. In Figure 10iii(F), assemblies of pure inulin are observed. On the extreme right (Figure 10iii(G)), OTAB-decorated inulin aggregates are found.

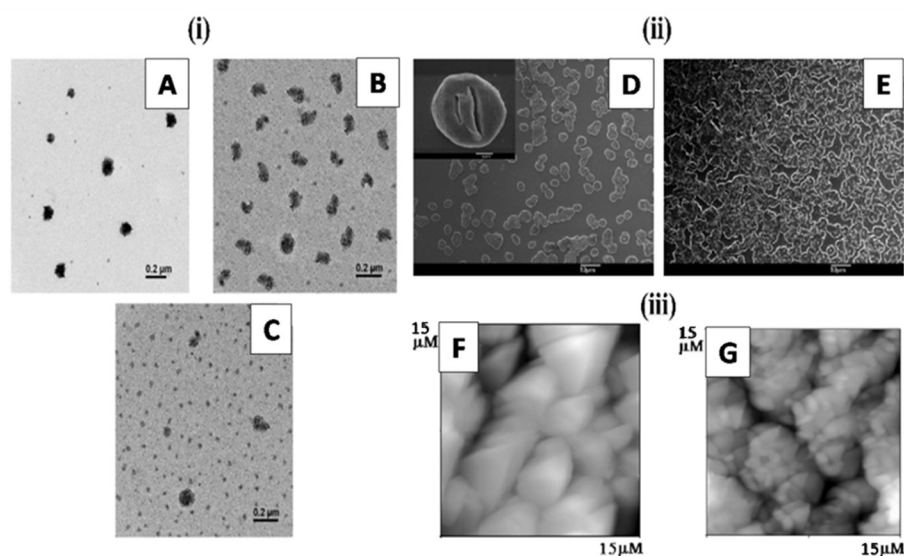


**Figure 10.** (i) TEM images of inulin without and with OTAB (octadecyl trimethyl ammonium bromide) are presented. (ii) FESEM demonstrations of the morphology change of inulin by the interaction with OTAB: (D) 0.5% ( $w/v$ ) pure inulin; (E) with  $[OTAB] > C_T$ . (iii) AFM images of pure inulin and the inulin–OTAB complex: (F) 0.5% ( $w/v$ ) pure inulin; (G) with  $[OTAB] > C_T$ . Reprinted with permission from *J. Phys. Chem. B*, 2009, 113, 8505. Copyright 2009 American Chemical Society.

Other relevant coacervation studies carried out in our laboratory were: (1) the interaction between a biotolerable, amino-acid-based amphiphile (*N*-dodecanoylsarcosinate, SDDS) and modified cationic polymers hydroxyethyl celluloses (JR 400 and LM 200) in isopropanol–water medium [116]; (2) a physicochemical study of the interaction of lysozyme with surface-active ionic liquid 1-butyl-3-methylimidazolium octyl sulfate

[BMIM][OS] in aqueous and buffer media [117]; (3) the physiochemistry of hexadecyl ammonium bromide and its methyl and ethanolic head group analogues in buffered aqueous and gelatin solution [118]; and (4) physicochemical studies on the interaction of gelatin with cationic surfactants alkyl trimethyl ammonium bromides (ATABs) with special focus on the behavior of the hexadecyl homologue [119]. Illustrations are not presented to save space; varied types of structures of the formed coacervates were observed. Kakizawa and Miyake [120] have shown the formation of coacervates by mixing oppositely charged polymers and detergents at certain concentrations. The electrostatic interaction between the two is considered as the driving force. The molecular structures of the components and their concentrations have an influence on the coacervation process. In shampoo, coacervate formation is based on the type of the alkyl ethoxylate sulfate (AES), the degree of cationization of the cellulose, and the coexisting electrolyte in the solution. The loose mesh-like morphology gives a smooth texture to the hair surface during rinsing. Coacervation in body wash is based on complexes of fatty acid salts with synthetic polymers, such as poly diallyldimethylammonium chloride having high adsorbability onto skin, and thereby contributes a moisturizing effect. Keshavarzi et al. [121] studied membrane formation by direct interaction in solution between biopolymers (Xanthan gum) and surfactants ( $C_n$ TAB,  $n = 10, 12, 14,$  and  $16$ ). A polymer–surfactant membrane spontaneously forms due to the precipitation of polymer–surfactant complexes in the medium. The polymer mass transfer is driven by the diffusion process along the concentration gradient. The surfactant hydrophobicity and concentration control the membrane structure and function. The properties of all the discussed polyelectrolyte/surfactant mixture coacervates can be explained by taking into consideration the molecular interactions that act between the polymer, and free and self-aggregate surfactants in solution. Hansson, for example, provided a thermodynamic theory for an aqueous solution of an oppositely charged polyion and surfactant complex [122]. Allen et al. [123] showed that the phase separation phenomenon for an opposite polymer–surfactant pair could be explained by a Poisson–Boltzmann cell model. In order to test this model, the phase behavior of the systems as well as molecular interactions within them must be studied.

### 5.2.3. Surfactant–Surfactant Types

In a study of the interaction between the catanionic system ( $C_{18}TA^+DS^-$ ) and the bovine serum albumin (BSA) in the solvent-spread monolayer in a buffered solution of pH (5.4), ionic strength of 0.01, and temperature of 298 K, we measured the surface pressure ( $\pi$ )–area isotherms in detail [124]. We revealed that at low  $\pi$ , BSA expands the coacervate/DPPC monolayer, while at high  $\pi$ , their protein-bound species are released into the subphase. The film morphologies studied by epifluorescence microscopy (EFM) (Figure 11a) revealed that the domains of both the DPPC and coacervate decreased in the presence of BSA. The average size of the circular domains of the pure catanionic system was 28  $\mu\text{m}$ , and 6  $\mu\text{m}$  in the presence of BSA. The presence of BSA in the coacervate/DPPC monolayer was also supported by AFM data analysis (Figure 11b). Here, the domains were homogeneously distributed with a mean height of 0.5 to 1 nm (top). The added BSA in the subphase penetrated into the monolayer through hydrophobic interaction, reducing the domain size and even forming dimers or trimers in the system.

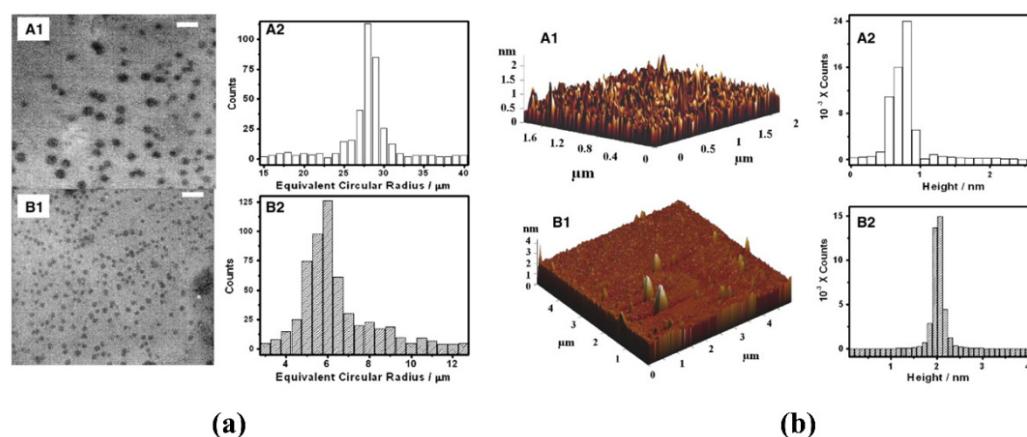


**Figure 11.** (a) Epifluorescence images of pure  $C_{18}TA^+DS^-$  (A1) and  $C_{18}TA^+DS^-BSA$  (B1) films ( $[BSA] = 0.25 \mu\text{g mL}^{-1}$ ) with their corresponding histograms at  $\pi = 25 \text{ mN m}^{-1}$  at  $\text{pH} = 5.4$  and  $T = 298 \text{ K}$ . Scale bar:  $100 \mu\text{m}$ . Total selected area (histogram):  $1900 \times 1400 \mu\text{m}$ . (b) AFM images of  $C_{18}TA^+DS^-$  in absence (A1) and presence of BSA ( $[BSA] = 0.25 \mu\text{g mL}^{-1}$ ) (B1) at different  $\pi$  with their corresponding histogram at  $298 \text{ K}$ . Total selected area (histogram):  $2 \times 2 \mu\text{m}$ . Reprinted with permission from *Materials Science and Engineering: C*, 2013, 33, 836. Copyright (2012) Elsevier B.V.

Douliez et al. [125] described the surfactant catanionic system of decanoic acid (DA) and a positively charged surfactant, either cetylpyridinium chloride (CPCI) or cetyltrimethylammonium bromide (CTAB) with the ability to form coacervates at  $\text{pH} 4.5\text{--}8.0$ , and  $30 \text{ mM}$  of DA and CPCI or CTAB in the presence of salts. The formed coacervates had spherical droplets with a dimension of  $5\text{--}50 \text{ nm}$ . The complex coacervates mainly consisted of elongated micelles. Biomolecules (e.g., enzymes and DNA) can easily be taken up and exchanged by this coacervate due to their catanionic nature.

#### 5.2.4. Peptide/Protein Types

The formation of simple and complex coacervates by a range of biological and synthetic polymers/macromolecules was covered in the preceding sections. Nevertheless, the frequently utilized synthetic and giant macromolecules used for coacervates are replaced by low-complexity peptides and proteins of specific importance from the perspective of protocells and the origin of life. These also have potential for protein stabilization, compartmentalization, and delivery.

Peptide length significantly affects how likely it is that they will coacervate [126]. Because the interactions are insufficient to overcome the mixing entropy below a threshold length, peptides do not phase-separate at a given temperature or salt concentration [127]. Perhaps even more significant than length is the charge density. Under physiological conditions, the threshold charge density for coacervation in peptides is around  $0.2$  per amino acid [128,129]. The external influencing factors ( $\text{pH}$ , ionic strength, temperature, solvent, etc.) can also significantly affect the protein- and peptide-based coacervation. Figure 12 illustrates various possible interactions involved in the formation of peptide-based coacervates.

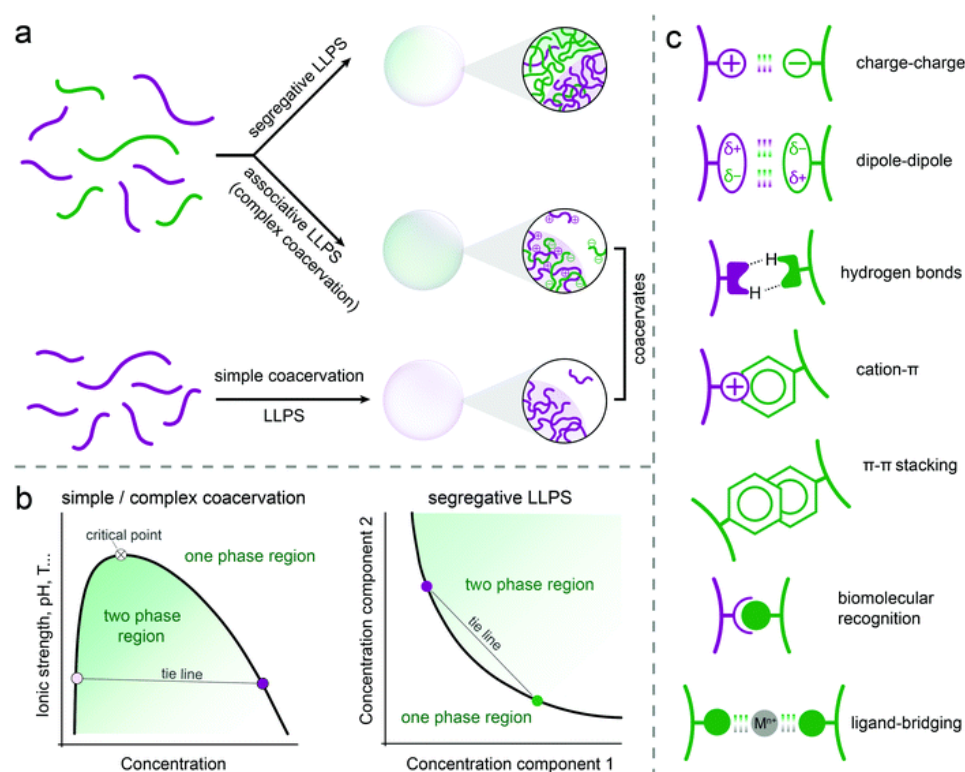


**Figure 12.** (a) Types of liquid–liquid phase separation (LLPS) and the formation of coacervates, (b) schematic phase diagrams of simple or complex coacervation and segregative phase separation, (c) possible interactions involved in the formation of peptide-based coacervates. Reprinted from *Chemical Society Review* 2021, 50, 3690–3705. Copyright 2021 Royal Society of Chemistry.

A fluorenylmethoxycarbonyl (Fmoc)-protected D-Ala-D-Ala dipeptide and a poly(diallyldimethylammonium chloride) (PDDA) complex coacervate system were described by Kumar et al. [130]. At pH 8, the combination was phase-separated into two liquid phases while the liquid coacervate droplets coarsened into fibrils as the pH steadily decreased, which is consistent with recent observations with the protein FUS. The deprotonation of Fmoc-AA peptide upon raising the pH could be used to reassemble droplets from the generated hydrogel as shown in Figure 13.

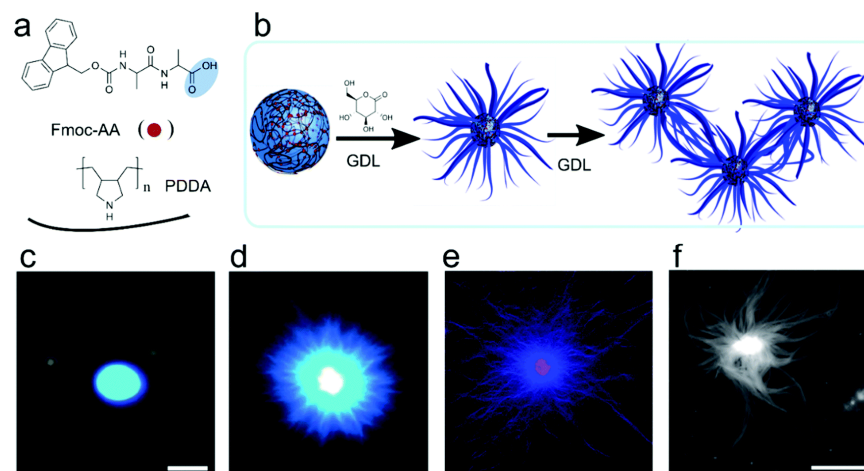


**Figure 13.** Chemical structures, schematic illustration, and microscopic images for the metamorphosis of coacervates–protocells to hydrogel, (a) chemical structures of dipeptide/polymer coacervate microdroplets prepared at pH 8.5, (b) schematic illustration of reconfiguration to aster-like core–shell microstructure at pH 4.5, (c,d) PDPA/Fmoc-AA coacervates before and after addition of GDL

(Glucono delta Lactone) and sequestered with Hoechst 33,258 fluorescent. This change from coacervates to nanofibers is induced due to the slow hydrolysis of GDL in the coacervates phase, (e) PDDA/Fmoc-AA coacervates core hydrogel sequestered with 1 mol% RITC-labelled PAH, (f) AFM images of nanofibrous gel. Reprinted from *Chemical Science* 2016, 7, 5879–5887. Copyright 2016 Royal Society of Chemistry.

There are numerous examples of peptides and proteins that separate solutions into a dense liquid phase under specific circumstances. The dense liquid phase can be a simple [131,132] or a complex coacervate [127,133]. Recently, Abbas et al. and Kapelner et al. reviewed in detail the formation of coacervates of proteins and peptides, respectively [134,135].

## 6. Applications of Coacervates

Coacervates are very useful in many facets of industry and biology. As mentioned earlier, they are used as medium for the synthesis of nanomaterials, as emulsifiers, in drug delivery, in cosmetic formulation (for example, body and skincare products), as additives in food processing, and viscosity modifiers. Complex coacervation has been used to drive ordered block copolymer gels, stimuli-responsive sensory materials, etc. It has been used for protein purification, wastewater treatment, and many others. Herein, we briefly discuss some uses and applications of coacervates.

### 6.1. Wastewater Treatment

The need for a cost-effective and environmentally as well as economically sustainable method of removing contaminants from large amounts of wastewater is very worthy of consideration. Coacervation-based extraction is widely used in the enrichment and separation of compounds from aqueous systems, and it has a number of advantages, including low organic-solvent consumption, nonvolatility and nonflammability, simple and time-/energy-/cost-effective procedures, and high extraction efficiency [136]. Surfactants are used in the majority of cases reported thus far.

Because of the potential toxicities of many surfactants, the use of alternative macromolecule-based coacervates has acquired interest in recent years. Immobilizing coacervate onto the porous solid surfaces to adsorb organic contaminants in wastewater is one of the ways. The coacervate of poly(diallyldimethylammonium chloride) (PDADMAC) with mixed low-toxic-surfactant micelles have been applied to glass and quartz sand, and have shown excellent interception of orange OT at high ionic strength [137]. Zhao et al. [138] developed a similar system from cationic gemini surfactant hexamethylene-1,6-bis(dodecyldimethylammonium bromide) and 10% hydrolyzed polyacrylamide (HPAM) in neutral conditions. The coacervates exhibit preferable adsorption of anionic methyl orange (MO) over cationic MB (methylene blue) due to the synergy of hydrophobic, electrostatic, and cation- $\pi$  interaction achieving an extraction efficiency of more than 95% with a polyacrylamide (PAM) concentration ranging from 0.05 to 0.5 wt.%. The coacervate formed by HPAM and a dynamic covalent cationic single-chain surfactant has also been used to recycle dyes in wastewater. Chiappisi et al. [139] showed that a highly pH-sensitive system based on cationic polysaccharide chitosan and the anionic surfactant nonoxyethyleneoleylether carboxylic acid can be used for the removal of dyes, metal ions, etc. Surfactant-free extraction systems are also the aim of development. Zhao and Zacharia [100] set three pairs of oppositely charged polyelectrolytes to generate complex coacervation, that is, cationic PEI and anionic poly(vinyl sulfonate), poly(acrylic acid) or poly(4-styrenesulfonic acid) (SPS), and compared their sequestration capacity for MB. As a result, only PEI/SPS showed good extraction efficiency (>80%) over a range of MB at its optimal pH ( $\approx 1.3$ ), while the other two pairs performed not so well, especially at low MB concentration. This indicated that electrostatic interaction, and the hydrophobic nature of the coacervate phase, might be insufficient to extract target compounds from the water-rich phase, and it is necessary to introduce other strong interactions such as  $\pi$ - $\pi$  interaction.

Recently, Valley et al. [140] reported that the coacervate of high-density inorganic polyoxometalate (POM) exhibits a fast phase-separation rate (within 1.0 min), low volume fraction, and high loading capacity for methylene blue (MB). Liu et al. [141] used trimeric cationic surfactant and negatively charged polyelectrolyte coacervate as a versatile approach for the removal of organic pollutants (Figure 14).

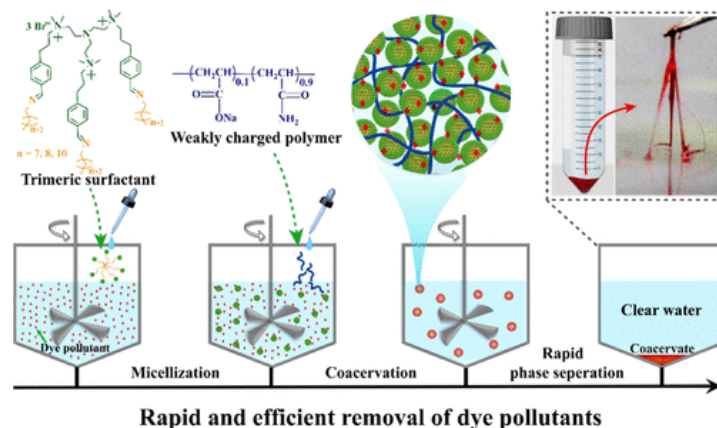


**Figure 14.** Schematic presentation of trimeric-surfactant-based coacervates for the removal of environmental pollutants. Reprinted with permission from *Langmuir*, 2021, 37, 5993. Copyright 2021 American Chemical Society.

Ballesteros-Gomez et al. showed that vesicular coacervates can be used for wastewater treatment [142]. Multifunctional supramolecular solvents (SUPRASs) were created in aqueous solutions comprising carboxylic acid and carboxylate combinations that self-assembled and coacervated when tetraalkylammonium ions were added. SUPRASs were made up of huge unilamellar vesicular aggregates connected by tetraalkylammonium ions in coacervate droplets. The SUPRASs produced were tested for their usefulness as multifunctional extractants in water treatment. At room temperature, the SUPRASs were found to remove all contaminants, including anionic, cationic, and ionizable dyes, as well as polyaromatic hydrocarbons (PAHs). The SUPRAS-based treatment was shown to be effective in removing colors from textile effluents and benzo(a) pyrene from tap water. SUPRASs, or coacervate droplets, have a great potential for use in complete wastewater treatment.

## 6.2. Protein Purification

Due to the many advantages mentioned in previous sections, coacervation-based purification has potential in a benign way without affecting the structure of the proteins. In this respect, complex coacervation has been considered a useful strategy. Proteins with low isoelectric pH ( $I_p$ ) favorably interact with cationic polyelectrolytes more than those with high  $I_p$ . The net charge of the protein is not the only factor. The surface charge duration (i.e., charge anisotropy) plays an important role [143,144]. From a 1:1 mixture of  $\beta$ -lactoglobulin (BLG,  $I_p \approx 5.2$ ) and bovine serum albumin (BSA,  $I_p \approx 4.9$ ), Xu et al. [145] extracted BLG employing cationic PDADMAC for its higher affinity to BLG than BSA in light of its negativity. At pH 7.0 and ionic strength = 0.1, the formed coacervate contained 90% BLG, and the associated polymer was totally removed by redissolution of the coacervate at pH 3.5, and subsequent ultrafiltration. Inverse protein selectivity has been realized with the anionic polysaccharide hyaluronic acid, the main difference being that coacervation is induced at pH 3.5 and dissolved at pH 7.0 [146]. In addition, the choice of polyelectrolytes can be extended to polysaccharides (chitosan and carrageenan) or protein (gelatin and lactoferrin) having biocompatibility for separating various protein mixtures including whey proteins, pea whey proteins, etc. [147–149]. Contributions of Kapelner and Obermeyer [150] and Lyons et al. [151] in this area, employing natural and model proteins of

varied amino acid sequences under different environmental conditions, can be referred to herein.

### 6.3. Food Formulation

Microencapsulation provides food systems with a variety of benefits, including the preservation of delicate agents in harsh environments, the extending of shelf life, the masking of disagreeable odors or tastes, the ease of handling and transportation, and so on [152]. Because of their nontoxicity, biocompatibility, and biodegradability, oppositely charged polysaccharides, proteins, etc., are commonly used as shell materials. The process usually consists of five steps: (i) dispersion of core materials in protein solution, (ii) creation of coacervate by adding polysaccharide solution, (iii) coacervate deposition around the core, (iv) hardening/crosslinking of the shell, and (v) drying of microcapsules into powders. Step (v) may be skipped in some cases. Many factors influence the size and appearance of the resulting microcapsules (e.g., formulation, temperature, pH, stirring rate, etc.). Mononuclear droplets, for example, form at low stirring rates, while multinuclear droplets form at high swirling rates [153,154].

The coacervation-based microencapsulation technology has been proven to be suitable for hydrophobic substances. Vanillin is a prevalent taste in dairy products; however, due to its volatile nature, it has a short shelf life. Hasanv and and Rafe [155] adopted  $\beta$ -cyclodextrin to afford an inclusion complex with vanillin first and then encapsulated it in the coacervate of rice bran protein and flaxseed gum. As a result, the rate of vanillin degradation was substantially slower, with the initial amount of vanillin staying at 75% after 30 days at room temperature. Nutritional oils are high in polyunsaturated fatty acids and have a variety of health benefits, although they are prone to oxidation. To address this issue, soya protein and chitosan were used by Yuan et al. [156] for encapsulating algal oil, considering that the coacervate shell shall function as a barrier to O<sub>2</sub> penetration where chitosan can function as a secondary oxidant. Additionally, oil-based microencapsulation of gelatin/cashew gum crosslinked by tannic acid, and gelatin/gum Arabic crosslinked by glutaraldehyde are reported [157,158]. Stable microcapsules of anchovy oil using gelatin and sodium hexametaphosphate were produced by Xia et al. [159].

Edible oils are found to be useful for increasing their partition in the coacervate phase. Rocha-Selmi et al. [160] employed both gum Arabic and gelatin to improve the heat resistance of aspartame. Calderón-Oliver et al. [161] studied the coacervate of collagen with pectin or alginate which was used to encapsulate antimicrobial peptide nisin, and antioxidant from avocado peel extract. At pH 3, the two shell matters showed different optimum protein–polysaccharide ratios (1:1 for collagen/alginate and 4:1 for collagen/pectin) although their encapsulation outcomes were nearly identical. Microorganisms such as probiotics are used in functional foods. Coacervate from gum Arabic and whey protein isolate was developed by Bosnea et al. [162] with reference to providing effective protection to live *L. Paracasei* cells in relation to yoghurt food production, and its storage in adverse environmental conditions. After 45 days at 4 °C, the polymer shell allowed the free passage of nutrients and metabolites for cell activity in the yogurt matrix, and about 97 percent cell viability was maintained. When cells were exposed to simulated stomach fluid (pH = 2) for 3 h, their survival was unaffected, and their decrease profile remained consistent throughout storage. Meanwhile, the integration of coacervate (3 wt.% polymers) with a concentration less than 10 wt.% appeared to have no effect on the rheological properties of yogurts, which is more appealing in practical applications.

### 6.4. Cellular Mimics

Coacervate is an abiotic cellular analog (i.e., protocell) with an ability to explore the mechanism of cell function, and related prebiotic evolution [163,164]. Compartmentalization provides benefits to different intracellular processes such as interior reaction rate and specificity, responding (1) to subtle environmental change, (2) inhibiting exterior reaction,

(3) buffering the concentration of the molecule, etc. [165,166]. A protocell comprising carboxymethyl dextran sodium salt and poly-*L*-lysine was created in relation to supporting RNA catalysis by Drobot et al. [167]. Kojima and Takayama [168] constructed coacervates using ATP and PDDA mixed with an aqueous two-phase system comprising dextran and PEG. The system showed a mitigation of substrate inhibition effect for dextranase. A ternary protocell consortia endowed with antagonistic enzyme-mediated interaction was designed by Qiao et al. [169]. The designed response–retaliation pathway has potential for programming population dynamics of interacting protocells.

Another significant problem in protocell production has been achieving reversible coacervation and disintegration as needed. In recent years, a variety of techniques have been examined, ranging from tuning external parameters such as temperature, pH, and ionic strength to manipulating phase-forming macromolecule concentration by synthesis and destruction, or their characteristics by post-translational modifications [170–172]. A complex coacervate using polyuridylic acid, RNA, and short cationic peptide was planned by Aumiller and Keating et al. [83], and thereby manipulated for phase separation by the enzymatic phosphorylation/dephosphorylation process. The assembly/disassembly behavior of the system-based single-stranded RNA and synthetic peptide was reported by Banerjee et al. [173]. They suggested a possible underlying supramolecular dynamical mechanism of ribonucleoprotein granules. Light-responsive coacervate droplets were prepared by Martin et al. [174] using double-stranded DNA and trans-azobenzene trimethylammonium bromide. The droplets breakdown under UV light and reassemble under blue light; the process is also thermal-sensitive. The photoswitchable protocell, when combined with the coacervate's ability to promote gene expression, could be used to trigger signaling pathways in populations.

### 6.5. Nanoparticle Synthesis

Coacervates have been found to be useful in the synthesis of nanoparticles. Nanoparticles are particles where at least one dimension of the particle is less than 100 nm. These particles have properties which are different from the corresponding bulk properties. The coassemblies of ionic-neutral block copolymers with oppositely charged species are called complex coacervate core micelles (C3Ms). These C3Ms can be used to synthesize nanoparticles because they are good nano reactors and scaffolds. Size and shape can be easily controlled. This is a straight forward, versatile synthetic method. These are water-based systems; organic solvents are not used and, hence, environmentally friendly. Metal, metal oxides, and quantum dots have been synthesized using C3Ms. The coacervate core can also be used for the biomimetic mineralization of silica, barium carbonate, and calcium carbonate [175]. The spherical, stable gelatin nanoparticles were prepared by Mohanty et al. [176] by using a simple coacervation process. Type B gelatin was used with ethanol as the coacervating liquid. Turbid solution was obtained which separated into two liquid phases. The upper supernatant dilute phase contained the gelatin nanoparticles which were characterized by dynamic light scattering, SANS, TEM, etc. Additionally, starch nanoparticles were prepared by addition of aqueous solution of synthesized positively charged (i.e., amine-group-containing) starch (PosSt) to aqueous solution of negatively charged (i.e., carboxylic-group-containing) charged starch (NegSt) under constant stirring at room temperature. Starch nanoparticles were formed spontaneously. These were characterized by particle size, size distribution (PDI), and  $\zeta$ -potential measurements. TEM was used for morphology determination. Particle sizes were 140 to 350 nm, and had a  $\zeta$ -potential ranging from  $-10$  to  $-35$  mV, depending on the formation conditions. The experimental details are available in original publication by Barthold et al. [177]. Gelatin nano-/submicron particles (GN/SPs) were synthesized using the binary nonsolvent-aided coacervation (BNAC) method. This coacervation method yields about a threefold lower particle size and higher average yield. In this study, 0.5% (*w/v*) gelatin aqueous solution with a binary nonsolvent system of acetone and ethanol was used. Particle size, zeta potential, swelling ratio, etc., were determined by Patra et al. [178].

### 6.6. Delivery Carrier

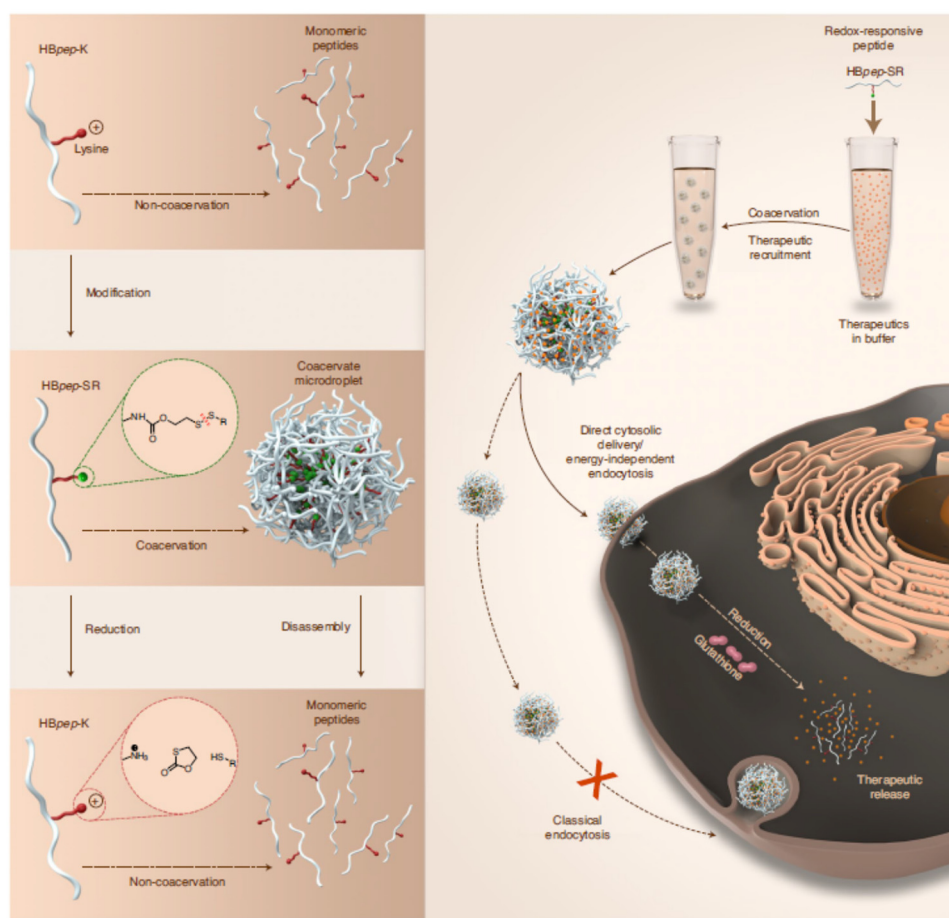
Complex coacervates used in controlled delivery systems are mostly in the form of either micro-/nanocapsules/beads or stimuli-responsive membranes for controlled delivery systems. As mentioned above [168], gelatin nanoparticles made by using the coacervation technique can be used for drug delivery. Nitrofurazone was used as a model drug to study drug-loading efficiency and its rate of release. The results indicate a potential for it in wound management. Barthold et al. [177] have shown that starch nanoparticles synthesized by the coacervation method can be used for the pulmonary delivery of proteins. Proteins which are “active pharmaceutical ingredient” such as Insulin, IgG1, RNase, etc., were used. Coacervate drug delivery is gaining momentum because of the controlled, sustained release of its cargo for long periods. Coacervates are also useful because both drug solubility and protein stability increase [179,180]. Different materials have been used as a platform for the delivery of drugs, proteins, RNA, DNA, and nutraceuticals.

Heparin forms coacervates with biodegradable polycation, poly (ethylene argininylnylaspartatediglyceride) (PEAD) and is a good carrier for growth factor (GF). These have high loading efficiency (>90%) and good bioactivity and biocompatibility; as it gives sustained release, the half-life increases and the administration of dose frequency decreases. Depending on the binding affinity of PEAD with heparin at various physiological conditions, the hydrolysis of PEAD can last for a few days to a month [181]. Injectable and biodegradable hydrogels, the entrapment medium, can be added to this which prolong the retention of coacervates in vivo [172]. The heparin/PEAD system has been widely used to deliver GF in case of heart repair, bone regeneration, wound healing, etc. [181–184]. Furthermore, “ibuprofen” was encapsulated in a system made of poly(allylamine hydrochloride) (PAH) and multivalent anion tripolyphosphate (TPP). The coacervate shows gel-like properties because of high electrostatic interaction. It has high load capacity and shows sustained release. The presence of sodium dodecylsulphate, however, makes the network permeable to small molecules making its release time tunable [185].

A UCST-type polymer was synthesized by Zhang et al. [186] by functionalizing a side group of poly(*N*-(2-hydroxypropyl)methacrylamide) with glycolamide, which formed a coacervate at decreasing temperatures from 50 °C to room temperature. The hydrophilic protein bovine serum albumin (BSA) could be accommodated in the formed coacervate. The coacervate, however, transformed to a soluble state with time and, hence, BSA was released in vivo over a period of four days.

Redox potential, pH, temperature, and glucose level are important considerations in determining targeted drug delivery platforms. The inflammatory and tumor sites are quite often acidic and, hence, one needs a pH-responsive system to target these sites. Nishida et al. [187] formed a pH-responsive LCST-type  $\beta$ -cyclodextrin-threaded polyrotaxane for the targeted delivery of therapeutic proteins. A glucose-responsive insulin delivery system is, again, very important. Insulin and glucose oxidase were incorporated in coacervate microdroplets with stable to neutral or alkaline pH. The insulin release rate was found to be a function of glucose level [188].

Cationic polymers with disulfide bonds can be grafted on dextran. This forms a coacervate with anionic gene plasmid. This coacervate is redox-responsive [189]. Sun et al. [190] discussed phase-separating peptides which can be used for cytosolic delivery and also the redox-activated release of macromolecular therapeutics (Scheme 4). Various macromolecules, small peptides, messenger RNA, etc., can be easily drafted within. This has great potential for cancer therapy as it is suitable for the delivery of siRNA which inhibits tumor growth.



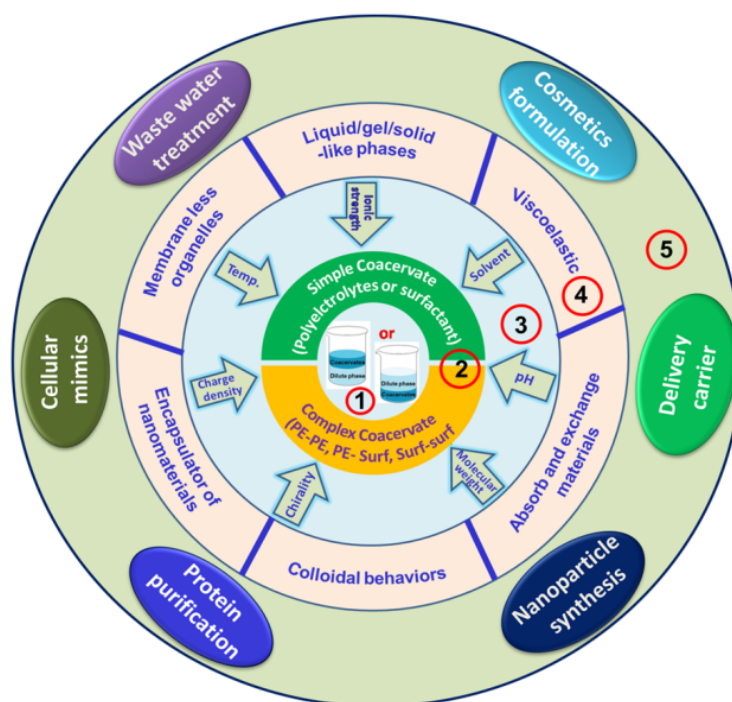
**Scheme 4.** Schematic fabrication of redox-responsive peptide coacervates with direct cytosolic entry that bypasses classical endocytosis. On incubation with cells, the therapeutics-loaded coacervates cross the cell membrane through an energy-independent endocytic pathway, possibly mediated by cholesterol-dependent lipid rafting, to migrate into the cytosol (bottom right), where they are reduced by GSH, resulting in the disassembly and release of the therapeutic). Reprinted from *Nat. Chem.* 2022, 14, 274. Copyright 2022 Nature Publishing Group.

pH-responsive carboxymethyl chitosan (CMCS) complex coacervate has been studied for oral drug delivery. The CMCS self-coacervates were made near its isoelectric point by adjusting pH. The FTIR results indicate the presence of electrostatic interactions, hydrogen bonding, and hydrophobic interactions in the CMCS self-coacervation, which remained stable in the pH range of 3.0–6.0. These coacervates were found to be pH-responsive and stable over a wide range of ionic strengths. Lactoferrin (LF) was encapsulated and used in oral delivery. The encapsulation efficiency was  $94.79 \pm 0.49\%$  with a loading capacity (LC) of  $26.29 \pm 0.52\%$  when 2 mg LF was present. Various experiments show that CMCS protects LF (>80%) from hydrolysis and remains bioactive [191].

## 7. Summary

The overview deals with some details of coacervates, the unique liquid phases comprising polymers, polyelectrolytes, proteins, and surfactants individually or in mixed states under the influences of environments including salts, solvents, temperature, pH, etc. A good number of simple and complex coacervates were chosen, and their properties and uses in practice were presented and discussed. Theories behind coacervation, and thermodynamic guidance therein, were described in brief along with their structures and physicochemical behaviors. The multifarious applications of the coacervates in the areas of water treatment, protein purification, food formation, cellular mimics, nanoparticle synthesis, etc., were concisely discussed.

An illustration (Scheme 5) of the aspects of coacervation and coacervates dealt with in the overview is presented below for readers' ready comprehension.



**Scheme 5.** A region-wise comprehensive presentation of different aspects of coacervation and coacervates. Regions: 1. Formed dense coacervates as the top or bottom phase; 2. Types of coacervates formed with examples; 3. Parameters influencing the coacervation process; 4. Important properties of coacervates; 5. Important applications of coacervates.

Coacervates were termed the associated phase of lipid-like bodies wherein the formation of life began in the 'primordial soup' about 4 billion years ago. However, no procedure has been thus far discovered which is in favor of life-bearing coacervate formation. There is no harm in being positive in this matter.

**Author Contributions:** Conceptualization: S.P.M., A.P. and B.N. Writing: S.P.M., A.K.R., A.P. and B.N. Revision and Editing: S.P.M., A.K.R. and B.N. Project administration: S.P.M., A.P. and B.N. All authors have read and agreed to the published version of the manuscript.

**Funding:** This research received no external funding.

**Acknowledgments:** SPM thanks the Indian National Science Academy and Jadavpur University for offering Emeritus Scientist and Emeritus Professorship, respectively. AKR acknowledges the Indian Society for Surface Science and Technology for supportive facilities. AP thanks the Department of Chemical Engineering at the University of Rhode Island for supporting this study. BN thanks Sundarban Hazi Desarat College for supportive facilities.

**Conflicts of Interest:** The authors declare no conflict of interest.

## References

1. Veis, A. A Review of the Early Development of the Thermodynamics of the Complex Coacervation Phase Separation. *Adv. Colloid Interface Sci.* **2011**, *167*, 2–11. <https://doi.org/10.1016/j.cis.2011.01.007>.
2. Kayitmazer, A.B. Thermodynamics of Complex Coacervation. *Adv. Colloid Interface Sci.* **2017**, *239*, 169–177. <https://doi.org/10.1016/j.cis.2016.07.006>.
3. Menger, F.M.; Sykes, B.M. Anatomy of a Coacervate. *Langmuir* **1998**, *14*, 4131–4137. <https://doi.org/10.1021/la980208m>.
4. Bungenberg De Jong, H.G.; Kruyt, H.R. Coacervation (partial miscibility in colloid systems). *Proc. K. Ned. Akad. Wet.* **1929**, *32*, 849–856.

5. Priftis, D.; Tirrell, M. Phase Behaviour and Complex Coacervation of Aqueous Polypeptide Solutions. *Soft Matter* **2012**, *8*, 9396–9405. <https://doi.org/10.1039/C2SM25604E>.
6. Sing, C.E. Development of the Modern Theory of Polymeric Complex Coacervation. *Adv. Colloid Interface Sci.* **2017**, *239*, 2–16. <https://doi.org/10.1016/j.cis.2016.04.004>.
7. Tiebackx, F.W. Gleichzeitige Ausflockung zweier Kolloide. *Zeitschr F Chem Und Ind Der Kolloide* **1911**, *8*, 198–201. <https://doi.org/10.1007/BF01503532>.
8. Fan, Y.; Wang, Y. Applications of Small-Angle X-ray Scattering/Small-Angle Neutron Scattering and Cryogenic Transmission Electron Microscopy to Understand Self-Assembly of Surfactants. *Curr. Opin. Colloid Interface Sci.* **2019**, *42*, 1–16. <https://doi.org/10.1016/j.cocis.2019.02.011>.
9. Kumar, D.; Steele, E.J.; Wickramasinghe, N.C. Preface: The origin of life and astrobiology. *Adv. Genet.* **2020**, *106*, xv–xviii. [https://doi.org/10.1016/S0065-2660\(20\)30037-7](https://doi.org/10.1016/S0065-2660(20)30037-7).
10. Oparin-Haldane Theory | Biology | Britannica. Available online: <https://www.britannica.com/science/Oparin-Haldane-theory> (accessed on 8 July 2022).
11. Zhou, M. The Origin of Life Discovered: ERNA. *OALib* **2018**, *5*, 1–15. <https://doi.org/10.4236/oalib.1104681>.
12. Tirard, S.J.B.S. Haldane and the Origin of Life. *J. Genet.* **2017**, *96*, 735–739. <https://doi.org/10.1007/s12041-017-0831-6>.
13. Ghosh, B.; Bose, B.; Dora, T.T.-Y. Can coacervation unify disparate hypotheses in the origin of cellular life? *Curr. Opin. Colloid Interface Sci.* **2021**, *52*, 101415. <https://doi.org/10.1016/j.cocis.2020.101415>.
14. Ivinova, O.N.; Izumrudov, V.A.; Muronetz, V.I.; Galaev, I.Yu.; Mattiasson, B. Influence of Complexing Polyanions on the Thermostability of Basic Proteins. *Macromol. Biosci.* **2003**, *3*, 210–215. <https://doi.org/10.1002/mabi.200390024>.
15. Hwang, D.S.; Zeng, H.; Srivastava, A.; Krogstad, D.V.; Tirrell, M.; Israelachvili, J.N.; Waite, J.H. Viscosity and Interfacial Properties in a Mussel-Inspired Adhesive Coacervate. *Soft Matter* **2010**, *6*, 3232–3236. <https://doi.org/10.1039/C002632H>.
16. Stewart, R.J.; Weaver, J.C.; Morse, D.E.; Waite, J.H. The Tube Cement of *Phragmatopoma Californica*: A Solid Foam. *J. Exp. Biol.* **2004**, *207*, 4727–4734. <https://doi.org/10.1242/jeb.01330>.
17. Kruyt, H.R.; Jackson, L.C. *Colloid Science Vol. II, Vol. II*; Elsevier Publ. Co: New York, NY, USA, 1949.
18. Zhao, W.; Wang, Y. Coacervation with Surfactants: From Single-Chain Surfactants to Gemini Surfactants. *Adv. Colloid Interface Sci.* **2017**, *239*, 199–212. <https://doi.org/10.1016/j.cis.2016.04.005>.
19. Ou, Z.; Muthukumar, M. Entropy and Enthalpy of Polyelectrolyte Complexation: Langevin Dynamics Simulations. *J. Chem. Phys.* **2006**, *124*, 154902. <https://doi.org/10.1063/1.2178803>.
20. Yu, S.; Xu, X.; Yigit, C.; Giet, M.; van der; Zidek, W.; Jankowski, J.; Dzubiella, J.; Ballauff, M. Interaction of Human Serum Albumin with Short Polyelectrolytes: A Study by Calorimetry and Computer Simulations. *Soft Matter* **2015**, *11*, 4630–4639. <https://doi.org/10.1039/C5SM00687B>.
21. Lytle, T.K.; Sing, C.E. Transfer Matrix Theory of Polymer Complex Coacervation. *Soft Matter* **2017**, *13*, 7001–7012. <https://doi.org/10.1039/C7SM01080J>.
22. Jho, Y.; Yoo, H.Y.; Lin, Y.; Han, S.; Hwang, D.S. Molecular and Structural Basis of Low Interfacial Energy of Complex Coacervates in Water. *Adv. Colloid Interface Sci.* **2017**, *239*, 61–73. <https://doi.org/10.1016/j.cis.2016.07.003>.
23. Ghasemi, M.; Larson, R.G. Future Directions in Physicochemical Modeling of the Thermodynamics of Polyelectrolyte Coacervates. *AIChE J.* **2022**, *68*, e17646. <https://doi.org/10.1002/aic.17646>.
24. Fu, J.; Schlenoff, J.B. Driving Forces for Oppositely Charged Polyion Association in Aqueous Solutions: Enthalpic, Entropic, but Not Electrostatic. *J. Am. Chem. Soc.* **2016**, *138*, 980–990. <https://doi.org/10.1021/jacs.5b11878>.
25. Zheng, B.; Avni, Y.; Andelman, D.; Podgornik, R. Phase Separation of Polyelectrolytes: The Effect of Charge Regulation. *J. Phys. Chem. B* **2021**, *125*, 7863–7870. <https://doi.org/10.1021/acs.jpcc.1c01986>.
26. Records, M.T., Jr.; Anderson, C.F.; Lohman, T.M. Thermodynamic analysis of ion effects on the binding and conformational equilibria of proteins and nucleic acids: The roles of ion association or release, screening and ion effects on water activity. *Q. Rev. Biophys.* **1978**, *11*, 103–178. <https://doi.org/10.1017/s003358350000202x>.
27. Mitra, D.; Chakraborty, I.; Bhattacharya, S.C.; Moulik, S.P. Interfacial and solution properties of tetraalkylammonium bromides and their sodium dodecylsulphate interacted products: A detailed physicochemical study. *Langmuir* **2007**, *23*, 3049–3061. <https://doi.org/10.1021/la062830h>.
28. Overbeek, J.T.; Voorn, M.J. Phase Separation in Polyelectrolyte Solutions; Theory of Complex Coacervation. *J. Cell. Physiol. Suppl.* **1957**, *49*, 7–22; discussion, 22–26.
29. Voorn, M.J. Complex Coacervation. III. Thermodynamic Calculations on Three-Component Systems. *Recl. Des. Trav. Chim. Des. Pays-Bas* **1956**, *75*, 427–446. <https://doi.org/10.1002/recl.19560750408>.
30. Flory, P.J. *Principles of Polymer Chemistry*; Cornell university press: Ithaca, NY, USA, 1953; ISBN 978-0-8014-0134-3.
31. Delaney, K.T.; Fredrickson, G.H. Theory of Polyelectrolyte Complexation—Complex Coacervates Are Self-Coacervates. *J. Chem. Phys.* **2017**, *146*, 224902. <https://doi.org/10.1063/1.4985568>.
32. Michaeli, I.; Overbeek, J.Th.G.; Voorn, M.J. Phase separation of polyelectrolyte solutions. *J. Polym. Sci.* **1957**, *23*, 443–450. <https://doi.org/10.1002/pol.1957.1202310337>.

33. Veis, A. Phase separation in polyelectrolyte solutions. II. interaction effects. *J. Phys. Chem.* **1961**, *65*, 1798–1803. <https://doi.org/10.1021/j100827a026>.
34. Nakajima, A.; Sato, H. Phase Relationships of an Equivalent Mixture of Sulfated Polyvinyl Alcohol and Aminoacetylated Polyvinyl Alcohol in Microsalt Aqueous Solution. *Biopolymers* **1972**, *11*, 1345–1355. <https://doi.org/10.1002/bip.1972.360110704>.
35. Sato, H.; Nakajima, A. Complex Coacervation in Sulfated Polyvinyl Alcohol-Amino Acetylated Polyvinyl Alcohol System. *Colloid Polym. Sci.* **1974**, *252*, 294–297. <https://doi.org/10.1007/BF01551150>.
36. Tainaka, K.-I. Effect of Counterions on Complex Coacervation. *Biopolymers* **1980**, *19*, 1289–1298. <https://doi.org/10.1002/bip.1980.360190705>.
37. Biesheuvel, P.M.; Cohen Stuart, M.A. Cylindrical Cell Model for the Electrostatic Free Energy of Polyelectrolyte Complexes. *Langmuir* **2004**, *20*, 4764–4770. <https://doi.org/10.1021/la0496789>.
38. Zhang, R.; Shklovskii, B.I. Phase Diagram of Solution of Oppositely Charged Polyelectrolytes. *Phys. A Stat. Mech. Its Appl.* **2005**, *352*, 216–238. <https://doi.org/10.1016/j.physa.2004.12.037>.
39. Borue, V.Yu.; Erukhimovich, I.Ya. A Statistical Theory of Globular Polyelectrolyte Complexes. *Macromolecules* **1990**, *23*, 3625–3632. <https://doi.org/10.1021/ma00217a015>.
40. Castelnovo, M.; Joanny, J.-F. Complexation between Oppositely Charged Polyelectrolytes: Beyond the Random Phase Approximation. *Eur. Phys. J. E* **2001**, *6*, 377–386. <https://doi.org/10.1007/s10189-001-8051-7>.
41. Kudlay, A.; Ermoshkin, A.V.; Olvera de la Cruz, M. Complexation of Oppositely Charged Polyelectrolytes: Effect of Ion Pair Formation. *Macromolecules* **2004**, *37*, 9231–9241. <https://doi.org/10.1021/ma048519t>.
42. Castelnovo, M.; Joanny, J.F. Phase Diagram of Diblock Polyampholyte Solutions. *Macromolecules* **2002**, *35*, 4531–4538. <https://doi.org/10.1021/ma012097v>.
43. Perry, S.L.; Sing, C.E. PRISM-Based Theory of Complex Coacervation: Excluded Volume versus Chain Correlation. *Macromolecules* **2015**, *48*, 5040–5053. <https://doi.org/10.1021/acs.macromol.5b01027>.
44. Lin, Y.-H.; Song, J.; Forman-Kay, J.D.; Chan, H.S. Random-Phase-Approximation Theory for Sequence-Dependent, Biologically Functional Liquid-Liquid Phase Separation of Intrinsically Disordered Proteins. *J. Mol. Liq.* **2017**, *228*, 176–193. <https://doi.org/10.1016/j.molliq.2016.09.090>.
45. Sing, C.E.; Perry, S.L. Recent Progress in the Science of Complex Coacervation. *Soft Matter* **2020**, *16*, 2885–2914. <https://doi.org/10.1039/D0SM00001A>.
46. Qin, J.; de Pablo, J.J. Criticality and Connectivity in Macromolecular Charge Complexation. *Macromolecules* **2016**, *49*, 8789–8800. <https://doi.org/10.1021/acs.macromol.6b02113>.
47. Rumyantsev, A.M.; de Pablo, J.J. Liquid Crystalline and Isotropic Coacervates of Semiflexible Polyanions and Flexible Polycations. *Macromolecules* **2019**, *52*, 5140–5156. <https://doi.org/10.1021/acs.macromol.9b00797>.
48. Priftis, D.; Xia, X.; Margossian, K.O.; Perry, S.L.; Leon, L.; Qin, J.; de Pablo, J.J.; Tirrell, M. Ternary, Tunable Polyelectrolyte Complex Fluids Driven by Complex Coacervation. *Macromolecules* **2014**, *47*, 3076–3085. <https://doi.org/10.1021/ma500245j>.
49. Chollakup, R.; Smitthipong, W.; Eisenbach, C.D.; Tirrell, M. Phase Behavior and Coacervation of Aqueous Poly(Acrylic Acid)–Poly(Allylamine) Solutions. *Macromolecules* **2010**, *43*, 2518–2528. <https://doi.org/10.1021/ma902144k>.
50. Perry, S.L.; Li, Y.; Priftis, D.; Leon, L.; Tirrell, M. The Effect of Salt on the Complex Coacervation of Vinyl Polyelectrolytes. *Polymers* **2014**, *6*, 1756–1772. <https://doi.org/10.3390/polym6061756>.
51. Fares, H.M.; Ghossoub, Y.E.; Delgado, J.D.; Fu, J.; Urban, V.S.; Schlenoff, J.B. Scattering Neutrons along the Polyelectrolyte Complex/Coacervate Continuum. *Macromolecules* **2018**, *51*, 4945–4955. <https://doi.org/10.1021/acs.macromol.8b00699>.
52. Wang, Q.; Schlenoff, J.B. The Polyelectrolyte Complex/Coacervate Continuum. *Macromolecules* **2014**, *47*, 3108–3116. <https://doi.org/10.1021/ma500500q>.
53. Radhakrishna, M.; Basu, K.; Liu, Y.; Shamsi, R.; Perry, S.L.; Sing, C.E. Molecular Connectivity and Correlation Effects on Polymer Coacervation. *Macromolecules* **2017**, *50*, 3030–3037. <https://doi.org/10.1021/acs.macromol.6b02582>.
54. Liu, Y.; Momani, B.; Winter, H.H.; Perry, S.L. Rheological Characterization of Liquid-to-Solid Transitions in Bulk Polyelectrolyte Complexes. *Soft Matter* **2017**, *13*, 7332–7340. <https://doi.org/10.1039/C7SM01285C>.
55. Ali, S.; Bleuel, M.; Prabhu, V.M. Lower Critical Solution Temperature in Polyelectrolyte Complex Coacervates. *ACS Macro Lett.* **2019**, *8*, 289–293. <https://doi.org/10.1021/acsmacrolett.8b00952>.
56. Wei, M.-T.; Elbaum-Garfinkle, S.; Holehouse, A.S.; Chen, C.C.-H.; Feric, M.; Arnold, C.B.; Priestley, R.D.; Pappu, R.V.; Brangwynne, C.P. Phase Behaviour of Disordered Proteins Underlying Low Density and High Permeability of Liquid Organelles. *Nat. Chem* **2017**, *9*, 1118–1125. <https://doi.org/10.1038/nchem.2803>.
57. Lou, J.; Friedowitz, S.; Qin, J.; Xia, Y. Tunable Coacervation of Well-Defined Homologous Polyanions and Polycations by Local Polarity. *ACS Cent. Sci.* **2019**, *5*, 549–557. <https://doi.org/10.1021/acscentsci.8b00964>.
58. Spruijt, E.; Westphal, A.H.; Borst, J.W.; Cohen Stuart, M.A.; van der Gucht, J. Binodal Compositions of Polyelectrolyte Complexes. *Macromolecules* **2010**, *43*, 6476–6484. <https://doi.org/10.1021/ma101031t>.
59. Li, L.; Srivastava, S.; Andreev, M.; Marciel, A.B.; de Pablo, J.J.; Tirrell, M.V. Phase Behavior and Salt Partitioning in Polyelectrolyte Complex Coacervates. *Macromolecules* **2018**, *51*, 2988–2995. <https://doi.org/10.1021/acs.macromol.8b00238>.

60. Fu, J.; Fares, H.M.; Schlenoff, J.B. Ion-Pairing Strength in Polyelectrolyte Complexes. *Macromolecules* **2017**, *50*, 1066–1074. <https://doi.org/10.1021/acs.macromol.6b02445>.
61. Sadman, K.; Wang, Q.; Chen, Y.; Keshavarz, B.; Jiang, Z.; Shull, K.R. Influence of Hydrophobicity on Polyelectrolyte Complexation. *Macromolecules* **2017**, *50*, 9417–9426. <https://doi.org/10.1021/acs.macromol.7b02031>.
62. Lim, S.; Moon, D.; Kim, H.J.; Seo, J.H.; Kang, I.S.; Cha, H.J. Interfacial Tension of Complex Coacervated Mussel Adhesive Protein According to the Hofmeister Series. *Langmuir* **2014**, *30*, 1108–1115. <https://doi.org/10.1021/la403680z>.
63. Spruijt, E.; Sprakel, J.; Stuart, M.A.C.; Gucht, J. van der Interfacial Tension between a Complex Coacervate Phase and Its Coexisting Aqueous Phase. *Soft Matter* **2009**, *6*, 172–178. <https://doi.org/10.1039/B911541B>.
64. Priftis, D.; Farina, R.; Tirrell, M. Interfacial Energy of Polypeptide Complex Coacervates Measured via Capillary Adhesion. *Langmuir* **2012**, *28*, 8721–8729. <https://doi.org/10.1021/la300769d>.
65. Sun, J.; Perry, S.L.; Schiffman, J.D. Electrospinning Nanofibers from Chitosan/Hyaluronic Acid Complex Coacervates. *Biomacromolecules* **2019**, *20*, 4191–4198. <https://doi.org/10.1021/acs.biomac.9b01072>.
66. Huang, J.; Morin, F.J.; Laaser, J.E. Charge-Density-Dominated Phase Behavior and Viscoelasticity of Polyelectrolyte Complex Coacervates. *Macromolecules* **2019**, *52*, 4957–4967. <https://doi.org/10.1021/acs.macromol.9b00036>.
67. Suarez-Martinez, P.C.; Batys, P.; Sannalokorpi, M.; Lutkenhaus, J.L. Time–Temperature and Time–Water Superposition Principles Applied to Poly(Allylamine)/Poly(Acrylic Acid) Complexes. *Macromolecules* **2019**, *52*, 3066–3074. <https://doi.org/10.1021/acs.macromol.8b02512>.
68. Heo, T.-Y.; Kim, S.; Chen, L.; Sokolova, A.; Lee, S.; Choi, S.-H. Molecular Exchange Kinetics in Complex Coacervate Core Micelles: Role of Associative Interaction. *ACS Macro Lett.* **2021**, *10*, 1138–1144. <https://doi.org/10.1021/acsmacrolett.1c00482>.
69. Markarian, M.Z.; Hariri, H.H.; Reisch, A.; Urban, V.S.; Schlenoff, J.B. A Small-Angle Neutron Scattering Study of the Equilibrium Conformation of Polyelectrolytes in Stoichiometric Saloplastic Polyelectrolyte Complexes. *Macromolecules* **2012**, *45*, 1016–1024. <https://doi.org/10.1021/ma2022666>.
70. Spruijt, E.; Leermakers, F.A.M.; Fokkink, R.; Schweins, R.; van Well, A.A.; Cohen Stuart, M.A.; van der Gucht, J. Structure and Dynamics of Polyelectrolyte Complex Coacervates Studied by Scattering of Neutrons, X-rays, and Light. *Macromolecules* **2013**, *46*, 4596–4605. <https://doi.org/10.1021/ma400132s>.
71. Joshi, N.; Rawat, K.; Bohidar, H.B. PH and Ionic Strength Induced Complex Coacervation of Pectin and Gelatin A. *Food Hydrocoll.* **2018**, *74*, 132–138. <https://doi.org/10.1016/j.foodhyd.2017.08.011>.
72. Kayitmazer, A.B.; Koksall, A.F.; Iyilik, E.K. Complex Coacervation of Hyaluronic Acid and Chitosan: Effects of PH, Ionic Strength, Charge Density, Chain Length and the Charge Ratio. *Soft Matter* **2015**, *11*, 8605–8612. <https://doi.org/10.1039/C5SM01829C>.
73. Chollakup, R.; Beck, J.B.; Dirnberger, K.; Tirrell, M.; Eisenbach, C.D. Polyelectrolyte Molecular Weight and Salt Effects on the Phase Behavior and Coacervation of Aqueous Solutions of Poly(Acrylic Acid) Sodium Salt and Poly(Allylamine) Hydrochloride. *Macromolecules* **2013**, *46*, 2376–2390. <https://doi.org/10.1021/ma202172q>.
74. Priftis, D.; Laugel, N.; Tirrell, M. Thermodynamic Characterization of Polypeptide Complex Coacervation. *Langmuir* **2012**, *28*, 15947–15957. <https://doi.org/10.1021/la302729r>.
75. Perry, S.L.; Leon, L.; Hoffmann, K.Q.; Kade, M.J.; Priftis, D.; Black, K.A.; Wong, D.; Klein, R.A.; Pierce, C.F.; Margossian, K.O.; et al. Chirality-Selected Phase Behaviour in Ionic Polypeptide Complexes. *Nat. Commun.* **2015**, *6*, 6052. <https://doi.org/10.1038/ncomms7052>.
76. Ali, S.; Prabhu, V.M. Relaxation behaviour by time-salt and time-temperature superposition of polyelectrolyte complexes from coacervate to precipitate. *Gels* **2018**, *4*, 11–22. <https://doi.org/10.3390/gels4010011>.
77. Kuroyanagi, S.; Shimada, N.; Fujii, S.; Furuta, T.; Harada, A.; Sakurai, K.; Maruyama, A. Highly Ordered Polypeptide with UCST Phase Separation Behavior. *J. Am. Chem. Soc.* **2019**, *141*, 1261–1268. <https://doi.org/10.1021/jacs.8b10168>.
78. Viereg, J.R.; Lueckheide, M.; Marciel, A.B.; Leon, L.; Bologna, A.J.; Rivera, J.R.; Tirrell, M.V. Oligonucleotide–Peptide Complexes: Phase Control by Hybridization. *J. Am. Chem. Soc.* **2018**, *140*, 1632–1638. <https://doi.org/10.1021/jacs.7b03567>.
79. Cummings, C.S.; Obermeyer, A.C. Phase Separation Behavior of Supercharged Proteins and Polyelectrolytes. *Biochemistry* **2018**, *57*, 314–323. <https://doi.org/10.1021/acs.biochem.7b00990>.
80. Aumiller, W.M.; Keating, C.D. Phosphorylation-Mediated RNA/Peptide Complex Coacervation as a Model for Intracellular Liquid Organelles. *Nat. Chem.* **2016**, *8*, 129–137. <https://doi.org/10.1038/nchem.2414>.
81. Anvari, M.; Pan, C.-H.; Yoon, W.-B.; Chung, D. Characterization of Fish Gelatin–Gum Arabic Complex Coacervates as Influenced by Phase Separation Temperature. *Int. J. Biol. Macromol.* **2015**, *79*, 894–902. <https://doi.org/10.1016/j.ijbiomac.2015.06.004>.
82. Kim, H.; Jeon, B.; Kim, S.; Jho, Y.; Hwang, D.S. Upper Critical Solution Temperature (UCST) Behavior of Coacervate of Cationic Protamine and Multivalent Anions. *Polymers* **2019**, *11*, 691. <https://doi.org/10.3390/polym11040691>.
83. Nakashima, K.K.; van Haren, M.H.I.; André, A.A.M.; Robu, I.; Spruijt, E. Active Coacervate Droplets Are Protocells That Grow and Resist Ostwald Ripening. *Nat. Commun.* **2021**, *12*, 3819. <https://doi.org/10.1038/s41467-021-24111-x>.
84. Sofronova, A.A.; Evstafyeva, D.B.; Izumrudov, V.A.; Muronetz, V.I.; Semenyuk, P.I. Protein–Polyelectrolyte Complexes: Molecular Dynamics Simulations and Experimental Study. *Polymer* **2017**, *113*, 39–45. <https://doi.org/10.1016/j.polymer.2017.02.047>.
85. Meng, S.; Liu, Y.; Yeo, J.; Ting, J.M.; Tirrell, M.V. Effect of mixed solvents on polyelectrolyte complexes with salt. *Colloid Polym. Sci.* **2020**, *298*, 887–894. <https://doi.org/10.1007/s00396-020-04637-0>.

86. Danielsen, S.P.O.; Nguyen, T.-Q.; Fredrickson, G.H.; Segalman, R.A. Complexation of a Conjugated Polyelectrolyte and Impact on Optoelectronic Properties. *ACS Macro Lett.* **2019**, *8*, 88–94. <https://doi.org/10.1021/acsmacrolett.8b00924>.
87. Khavani, M.; Batys, P.; Lalwani, S.M.; Eneh, C.I.; Leino, A.; Lutkenhaus, J.L.; Sammalkorpi, M. Effect of Ethanol and Urea as Solvent Additives on PSS–PDADMA Polyelectrolyte Complexation. *Macromolecules* **2022**, *55*, 3140–3150. <https://doi.org/10.1021/acs.macromol.1c02533>.
88. Zhou, L.; Fan, Y.; Liu, Z.; Chen, L.; Spruijt, E.; Wang, Y. A Multiresponsive Transformation between Surfactant-Based Coacervates and Vesicles. *CCS Chem.* **2021**, *3*, 358–366. <https://doi.org/10.31635/ccschem.021.202000702>.
89. Menger, F.M.; Seredyuk, V.A.; Apkarian, R.P.; Wright, E.R. Colloidal Assemblies of Branched Geminis Studied by Cryo-Etch-HRSEM. *J. Am. Chem. Soc.* **2002**, *124*, 12408–12409. <https://doi.org/10.1021/ja021025w>.
90. Huang, X.; Cao, M.; Wang, J.; Wang, Y. Controllable Organization of a Carboxylic Acid Type Gemini Surfactant at Different PH Values by Adding Copper(II) Ions. *J. Phys. Chem. B* **2006**, *110*, 19479–19486. <https://doi.org/10.1021/jp0630121>.
91. Mohanty, B.; Bohidar, H.B. Systematic of Alcohol-Induced Simple Coacervation in Aqueous Gelatin Solutions. *Biomacromolecules* **2003**, *4*, 1080–1086. <https://doi.org/10.1021/bm034080l>.
92. Manaf, M.A.; Subuki, I.; Jai, J.; Raslan, R.; Mustapa, A.N. Encapsulation of Volatile Citronella Essential Oil by Coacervation: Efficiency and Release Study. *IOP Conf. Ser. Mater. Sci. Eng.* **2018**, *358*, 012072. <https://doi.org/10.1088/1757-899X/358/1/012072>.
93. Perro, A.; Giraud, L.; Coudon, N.; Shanmugathasan, S.; Lapeyre, V.; Goudeau, B.; Douliez, J.-P.; Ravaine, V. Self-Coacervation of Ampholyte Polymer Chains as an Efficient Encapsulation Strategy. *J. Colloid Interface Sci* **2019**, *548*, 275–283. <https://doi.org/10.1016/j.jcis.2019.04.033>.
94. Lazko, J.; Popineau, Y.; Legrand, J. Soy Glycinin Microcapsules by Simple Coacervation Method. *Colloids Surf. B: Biointerfaces* **2004**, *37*, 1–8. <https://doi.org/10.1016/j.colsurfb.2004.06.004>.
95. Rizvi, A.; Patel, U.; Ianiro, A.; Hurst, P.J.; Merham, J.G.; Patterson, J.P. Nonionic Block Copolymer Coacervates. *Macromolecules* **2020**, *53*, 6078–6086. <https://doi.org/10.1021/acs.macromol.0c00979>.
96. Chen, N.; Zhao, Z.; Wang, Y.; Dimova, R. Resolving the Mechanisms of Soy Glycinin Self-Coacervation and Hollow-Condensate Formation. *ACS Macro Lett.* **2020**, *9*, 1844–1852. <https://doi.org/10.1021/acsmacrolett.0c00709>.
97. Burke, N.A.D.; Mazumder, M.A.J.; Hanna, M.; Stöver, H.D.H. Polyelectrolyte Complexation between Poly(Methacrylic Acid, Sodium Salt) and Poly(Diallyldimethylammonium Chloride) or Poly [2-(Methacryloyloxyethyl) Trimethylammonium Chloride]. *J. Polym. Sci. Part A Polym. Chem.* **2007**, *45*, 4129–4143. <https://doi.org/10.1002/pola.22247>.
98. Lappan, U.; Scheler, U. Influence of the Nature of the Ion Pairs on the Segmental Dynamics in Polyelectrolyte Complex Coacervate Phases. *Macromolecules* **2017**, *50*, 8631–8636. <https://doi.org/10.1021/acs.macromol.7b01858>.
99. Salehi, A.; Desai, P.S.; Li, J.; Steele, C.A.; Larson, R.G. Relationship between Polyelectrolyte Bulk Complexation and Kinetics of Their Layer-by-Layer Assembly. *Macromolecules* **2015**, *48*, 400–409. <https://doi.org/10.1021/ma502273a>.
100. Zhao, M.; Zacharia, N.S. Sequestration of Methylene Blue into Polyelectrolyte Complex Coacervates. *Macromol. Rapid Commun.* **2016**, *37*, 1249–1255. <https://doi.org/10.1002/marc.201600244>.
101. Vitorazi, L.; Ould-Moussa, N.; Sekar, S.; Fresnais, J.; Loh, W.; Chapel, J.-P.; Berret, J.-F. Evidence of a Two-Step Process and Pathway Dependency in the Thermodynamics of Poly(Diallyldimethylammonium Chloride)/Poly(Sodium Acrylate) Complexation. *Soft Matter* **2014**, *10*, 9496–9505. <https://doi.org/10.1039/C4SM01461H>.
102. Kayitmazer, A.B.; Strand, S.P.; Tribet, C.; Jaeger, W.; Dubin, P.L. Effect of Polyelectrolyte Structure on Protein–Polyelectrolyte Coacervates: Coacervates of Bovine Serum Albumin with Poly(Diallyldimethylammonium Chloride) versus Chitosan. *Biomacromolecules* **2007**, *8*, 3568–3577. <https://doi.org/10.1021/bm700645t>.
103. Leisner, D.; Imae, T. Interpolyelectrolyte Complex and Coacervate Formation of Poly(Glutamic Acid) with a Dendrimer Studied by Light Scattering and SAXS. *J. Phys. Chem. B* **2003**, *107*, 8078–8087. <https://doi.org/10.1021/jp027365l>.
104. Li, H.; Fauquignon, M.; Haddou, M.; Schatz, C.; Chapel, J.-P. Interfacial Behavior of Solid- and Liquid-like Polyelectrolyte Complexes as a Function of Charge Stoichiometry. *Polymers* **2021**, *13*, 3848. <https://doi.org/10.3390/polym13213848>.
105. Yang, M.; Digby, Z.A.; Schlenoff, J.B. Precision Doping of Polyelectrolyte Complexes: Insight on the Role of Ions. *Macromolecules* **2020**, *53*, 5465–5474. <https://doi.org/10.1021/acs.macromol.0c00965>.
106. Swanson, J.P.; Monteleone, L.R.; Haso, F.; Costanzo, P.J.; Liu, T.; Joy, A. A Library of Thermoresponsive, Coacervate-Forming Biodegradable Polyesters. *Macromolecules* **2015**, *48*, 3834–3842. <https://doi.org/10.1021/acs.macromol.5b00585>.
107. Cruz, M.A.; Morris, D.L.; Swanson, J.P.; Kundu, M.; Mankoci, S.G.; Leeper, T.C.; Joy, A. Efficient Protein Encapsulation within Thermoresponsive Coacervate-Forming Biodegradable Polyesters. *ACS Macro Lett.* **2018**, *7*, 477–481. <https://doi.org/10.1021/acsmacrolett.8b00118>.
108. Kundu, M.; Morris, D.L.; Cruz, M.A.; Miyoshi, T.; Leeper, T.C.; Joy, A. Elucidating the Molecular Interactions of Encapsulated Doxorubicin within a Nonionic, Thermoresponsive Polyester Coacervate. *ACS Appl. Bio Mater.* **2020**, *3*, 4626–4634. <https://doi.org/10.1021/acsabm.0c00507>.
109. Narayanan, A.; Menefee, J.R.; Liu, Q.; Dhinojwala, A.; Joy, A. Lower Critical Solution Temperature-Driven Self-Coacervation of Nonionic Polyester Underwater Adhesives. *ACS Nano* **2020**, *14*, 8359–8367. <https://doi.org/10.1021/acsnano.0c02396>.
110. Li, Y.; Dubin, P.L.; Havel, H.A.; Edwards, S.L.; Dautzenberg, H. Complex Formation between Polyelectrolyte and Oppositely Charged Mixed Micelles: Soluble Complexes vs. Coacervation. *Langmuir* **1995**, *11*, 2486–2492. <https://doi.org/10.1021/la00007a029>.

111. Kizilay, E.; Dinsmore, A.D.; Hoagland, D.A.; Sun, L.; Dubin, P.L. Evolution of Hierarchical Structures in Polyelectrolyte–Micelle Coacervates. *Soft Matter* **2013**, *9*, 7320–7332. <https://doi.org/10.1039/C3SM50591J>.
112. Wang, Y.; Kimura, K.; Dubin, P.L.; Jaeger, W. Polyelectrolyte–Micelle Coacervation: Effects of Micelle Surface Charge Density, Polymer Molecular Weight, and Polymer/Surfactant Ratio. *Macromolecules* **2000**, *33*, 3324–3331. <https://doi.org/10.1021/ma991886y>.
113. Kizilay, E.; Maccarrone, S.; Foun, E.; Dinsmore, A.D.; Dubin, P.L. Cluster Formation in Polyelectrolyte–Micelle Complex Coacervation. *J. Phys. Chem. B* **2011**, *115*, 7256–7263. <https://doi.org/10.1021/jp109788r>.
114. Dan, A.; Ghosh, S.; Moulik, S.P. Interaction of Cationic Hydroxyethylcellulose (JR400) and Cationic Hydrophobically Modified Hydroxyethylcellulose (LM200) with the Amino-Acid Based Anionic Amphiphile Sodium N-Dodecanoyl Sarcosinate(SDDS) in Aqueous Medium. *Carbohydr. Polym.* **2010**, *80*, 44–52. <https://doi.org/10.1016/j.carbpol.2009.10.061>.
115. Dan, A.; Ghosh, S.; Moulik, S.P. Physicochemistry of the Interaction between Inulin and Alkyltrimethylammonium Bromides in Aqueous Medium and the Formed Coacervates. *J. Phys. Chem. B* **2009**, *113*, 8505–8513. <https://doi.org/10.1021/jp902641d>.
116. Mandal, B.; Ghosh, S.; Moulik, S.P. Interaction between a Bio-Tolerable Amino-Acid Based Amphiphile (N-Dodecanoylsarcosinate, SDDS) and Modified Cationic Polymers, Hydroxyethylcelluloses (JR 400, and LM 200) in Isopropanol-Water Medium. *Colloids Surf. A Physicochem. Eng. Asp.* **2019**, *566*, 156–165. <https://doi.org/10.1016/j.colsurfa.2019.01.002>.
117. Mandal, B.; Mondal, S.; Pan, A.; Moulik, S.P.; Ghosh, S. Physicochemical Study of the Interaction of Lysozyme with Surface Active Ionic Liquid 1-Butyl-3-Methylimidazolium Octylsulfate [BMIM] [OS] in Aqueous and Buffer Media. *Colloids Surf. A Physicochem. Eng. Asp.* **2015**, *484*, 345–353. <https://doi.org/10.1016/j.colsurfa.2015.07.052>.
118. Mitra, D.; Bhattacharya, S.C.; Moulik, S.P. Physicochemical Studies on the Interaction of Gelatin with Cationic Surfactants Alkyltrimethylammonium Bromides (ATABs) with Special Focus on the Behavior of the Hexadecyl Homologue. *J. Phys. Chem. B* **2008**, *112*, 6609–6619. <https://doi.org/10.1021/jp800320a>.
119. Mitra, D.; Moulik, S.P. Physicochemistry of Hexadecylammonium Bromide and Its Methyl and Ethanolic Head Group Analogues in Buffered Aqueous and Gelatin Solution. *J. Chem. Sci.* **2010**, *122*, 349–362. <https://doi.org/10.1007/s12039-010-0040-9>.
120. Kakizawa, Y.; Miyake, M. Creation of New Functions by Combination of Surfactant and Polymer—Complex Coacervation with Oppositely Charged Polymer and Surfactant for Shampoo and Body Wash. *J. Oleo Sci.* **2019**, *68*, 525–539. <https://doi.org/10.5650/jos.ess19081>.
121. Keshavarzi, B.; Schwarzenberger, K.; Huang, M.; Javadi, A.; Eckert, K. Formation of Structured Membranes by Coacervation of Xanthan Gum with CnTAB Surfactants. *Langmuir* **2019**, *35*, 13624–13635. <https://doi.org/10.1021/acs.langmuir.9b02220>.
122. Hansson, P. Phase Behavior of Aqueous Polyion–Surfactant Ion Complex Salts: A Theoretical Analysis. *J. Colloid Interface Sci.* **2009**, *332*, 183–193. <https://doi.org/10.1016/j.jcis.2008.12.011>.
123. Allen, R.J.; Warren, P.B. Phase Behaviour of Oppositely Charged Polymer/Surfactant Mixtures. *EPL* **2003**, *64*, 468. <https://doi.org/10.1209/epl/i2003-00234-2>.
124. Maiti, K.; Bhattacharya, S.C.; Moulik, S.P.; Panda, A.K. Effect of Bovine Serum Albumin on the Functionality and Structure of Catanionic Surfactant at Air–Buffer Interface. *Mater. Sci. Eng. C* **2013**, *33*, 836–843. <https://doi.org/10.1016/j.msec.2012.11.009>.
125. Douliez, J.-P.; Martin, N.; Gaillard, C.; Beneyton, T.; Baret, J.-C.; Mann, S.; Beven, L. Catanionic Coacervate Droplets as a Surfactant-Based Membrane-Free Protocell Model. *Angew. Chem. Int. Ed.* **2017**, *56*, 13689–13693. <https://doi.org/10.1002/anie.201707139>.
126. Dzuricky, M.; Rogers, B.A.; Shahid, A.; Cremer, P.S.; Chilkoti, A. De novo engineering of intracellular condensates using artificial disordered proteins. *Nat. Chem.* **2020**, *12*, 814–825. <https://doi.org/10.1038/s41557-020-0511-7>.
127. Cakmak, F.P.; Choi, S.; Meyer, M.O.; Bevilacqua, P.C.; Keating, C.D. rebiotically-relevant low polyion multivalency can improve functionality of membraneless compartments. *Nat. Commun.* **2020**, *11*, 5949. <https://doi.org/10.1038/s41467-020-19775-w>.
128. Te Brinke, E.; Groen, J.; Herrmann, A.; Heus, H.A.; Rivas, G.; Spruijt, E.; Huck, W.T.S. Dissipative adaptation in driven self-assembly leading to self-dividing fibrils. *Nat. Nanotechnol.* **2018**, *13*, 849–855. <https://doi.org/10.1038/s41565-018-0192-1>.
129. Ma, C.; Malessa, A.; Boersma, A.J.; Liu, K.; Herrmann, A. Supercharged Proteins and Polypeptides. *Adv. Mater.* **2020**, *32*, e1905309. <https://doi.org/10.1002/adma.201905309>.
130. Kumar, R.K.; Harniman, R.L.; Patil, A.J.; Mann, S. Self-transformation and structural reconfiguration in coacervate-based protocells. *Chem. Sci.* **2016**, *7*, 5879–5887. <https://doi.org/10.1039/C6SC00205F>.
131. Gabryelczyk, B.; Cai, H.; Shi, X.; Sun, Y.; Swinkels, P.J.M.; Salentinig, S.; Pervushin, K.; Miserez, A. Hydrogen bond guidance and aromatic stacking drive liquid-liquid phase separation of intrinsically disordered histidine-rich peptides. *Nat. Commun.* **2019**, *10*, 5465. <https://doi.org/10.1038/s41467-019-13469-8>.
132. Wei, W.; Petrone, L.; Tan, Y.; Cai, H.; Israelachvili, J.N.; Miserez, A.; Waite, J.H. An Underwater Surface-Drying Peptide Inspired by a Mussel Adhesive Protein. *Adv. Funct. Mater.* **2016**, *26*, 3496–3507. <https://doi.org/10.1002/adfm.201600210>.
133. Koga, S.; Williams, D.S.; Perriman, A.W.; Mann, S. Peptide-nucleotide microdroplets as a step towards a membrane-free protocell model. *Nat. Chem.* **2011**, *3*, 720–724. <https://doi.org/10.1038/nchem.1110>.
134. Abbas, M.; Lipin’ski, W.P.; Wang, J.; Spruijt, E. Peptide-based coacervates as biomimetic Protocells. *Chem. Soc. Rev.* **2021**, *50*, 3690–3705. <https://doi.org/10.1039/d0cs00307g>.
135. Kapelner, R.A.; Yeong, V.; Obermeyer, A.C. Molecular determinants of protein-based coacervates. *Curr. Opin. Colloid Interface Sci.* **2021**, *52*, 10140. <https://doi.org/10.1016/j.cocis.2020.101407>.

136. Melnyk, A.; Namieśnik, J.; Wolska, L. Theory and Recent Applications of Coacervate-Based Extraction Techniques. *TrAC Trends Anal. Chem.* **2015**, *71*, 282–292. <https://doi.org/10.1016/j.trac.2015.03.013>.
137. Wang, Y.; Banziger, J.; Dubin, P.L.; Filippelli, G.; Nuraje, N. Adsorptive Partitioning of an Organic Compound onto Polyelectrolyte-Immobilized Micelles on Porous Glass and Sand. *Environ. Sci. Technol.* **2001**, *35*, 2608–2611. <https://doi.org/10.1021/es001662r>.
138. Zhao, W.; Fan, Y.; Wang, H.; Wang, Y. Coacervate of Polyacrylamide and Cationic Gemini Surfactant for the Extraction of Methyl Orange from Aqueous Solution. *Langmuir* **2017**, *33*, 6846–6856. <https://doi.org/10.1021/acs.langmuir.7b01421>.
139. Chiappisi, L.; Simon, M.; Gradzielski, M. Toward Bioderived Intelligent Nanocarriers for Controlled Pollutant Recovery and PH-Sensitive Binding. *ACS Appl. Mater. Interfaces* **2015**, *7*, 6139–6145. <https://doi.org/10.1021/am508846r>.
140. Valley, B.; Jing, B.; Ferreira, M.; Zhu, Y. Rapid and Efficient Coacervate Extraction of Cationic Industrial Dyes from Wastewater. *ACS Appl. Mater. Interfaces* **2019**, *11*, 7472–7478. <https://doi.org/10.1021/acsami.8b21674>.
141. Liu, B.; Zhao, W.; Shen, Y.; Fan, Y.; Wang, Y. Trimeric Cationic Surfactant Coacervation as a Versatile Approach for Removing Organic Pollutants. *Langmuir* **2021**, *37*, 5993–6001. <https://doi.org/10.1021/acs.langmuir.1c00557>.
142. Ballesteros-Gómez, A.; Caballero-Casero, N.; García-Fonseca, S.; Lunar, L.; Rubio, S. Multifunctional Vesicular Coacervates as Engineered Supramolecular Solvents for Wastewater Treatment. *Chemosphere* **2019**, *223*, 569–576. <https://doi.org/10.1016/j.chemosphere.2019.02.089>.
143. Sieberz, J.; Wohlgemuth, K.; Schembecker, G. The Influence of Impurity Proteins on the Precipitation of a Monoclonal Antibody with an Anionic Polyelectrolyte. *Sep. Purif. Technol.* **2015**, *146*, 252–260. <https://doi.org/10.1016/j.seppur.2015.03.055>.
144. Xu, Y.; Liu, M.; Faisal, M.; Si, Y.; Guo, Y. Selective Protein Complexation and Coacervation by Polyelectrolytes. *Adv. Colloid Interface Sci.* **2017**, *239*, 158–167. <https://doi.org/10.1016/j.cis.2016.06.004>.
145. Xu, Y.; Mazzawi, M.; Chen, K.; Sun, L.; Dubin, P.L. Protein Purification by Polyelectrolyte Coacervation: Influence of Protein Charge Anisotropy on Selectivity. *Biomacromolecules* **2011**, *12*, 1512–1522. <https://doi.org/10.1021/bm101465y>.
146. Du, X.; Dubin, P.L.; Hoagland, D.A.; Sun, L. Protein-Selective Coacervation with Hyaluronic Acid. *Biomacromolecules* **2014**, *15*, 726–734. <https://doi.org/10.1021/bm500041a>.
147. Yang, S.; Li, X.; Hua, Y.; Chen, Y.; Kong, X.; Zhang, C. Selective Complex Coacervation of Pea Whey Proteins with Chitosan To Purify Main 2S Albumins. *J. Agric. Food Chem.* **2020**, *68*, 1698–1706. <https://doi.org/10.1021/acs.jafc.9b06311>.
148. Pathak, J.; Rawat, K.; Aswal, V.K.; Bohidar, H.B. Interactions in Globular Proteins with Polyampholyte: Coacervation Route for Protein Separation. *RSC Adv.* **2015**, *5*, 13579–13589. <https://doi.org/10.1039/C4RA13133A>.
149. Tavares, G.M.; Croguennec, T.; Hamon, P.; Carvalho, A.F.; Bouhallab, S. Selective Coacervation between Lactoferrin and the Two Isoforms of  $\beta$ -Lactoglobulin. *Food Hydrocoll.* **2015**, *48*, 238–247. <https://doi.org/10.1016/j.foodhyd.2015.02.027>.
150. A.Kapelner, R.; C.Obermeyer, A. Ionic Polypeptide Tags for Protein Phase Separation. *Chem. Sci.* **2019**, *10*, 2700–2707. <https://doi.org/10.1039/C8SC04253E>.
151. Lyons, R.E.; Elvin, C.M.; Taylor, K.; Lekieffre, N.; Ramshaw, J.A.M. Purification of Recombinant Protein by Cold-Coacervation of Fusion Constructs Incorporating Resilin-Inspired Polypeptides. *Biotechnol. Bioeng.* **2012**, *109*, 2947–2954. <https://doi.org/10.1002/bit.24565>.
152. Devi, N.; Sarmah, M.; Khatun, B.; Maji, T.K. Encapsulation of Active Ingredients in Polysaccharide-Protein Complex Coacervates. *Adv. Colloid Interface Sci.* **2017**, *239*, 136–145. <https://doi.org/10.1016/j.cis.2016.05.009>.
153. Timilsena, Y.P.; Akanbi, T.O.; Khalid, N.; Adhikari, B.; Barrow, C.J. Complex Coacervation: Principles, Mechanisms and Applications in Microencapsulation. *Int. J. Biol. Macromol.* **2019**, *121*, 1276–1286. <https://doi.org/10.1016/j.ijbiomac.2018.10.144>.
154. Eghbal, N.; Choudhary, R. Complex Coacervation: Encapsulation and Controlled Release of Active Agents in Food Systems. *LWT* **2018**, *90*, 254–264. <https://doi.org/10.1016/j.lwt.2017.12.036>.
155. Hasanvand, E.; Rafe, A. Development of Vanillin/ $\beta$ -Cyclodextrin Inclusion Microcapsules Using Flax Seed Gum-Rice Bran Protein Complex Coacervates. *Int. J. Biol. Macromol.* **2019**, *131*, 60–66. <https://doi.org/10.1016/j.ijbiomac.2019.03.066>.
156. Yuan, Y.; Kong, Z.-Y.; Sun, Y.-E.; Zeng, Q.-Z.; Yang, X.-Q. Complex Coacervation of Soy Protein with Chitosan: Constructing Antioxidant Microcapsule for Algal Oil Delivery. *LWT* **2017**, *75*, 171–179. <https://doi.org/10.1016/j.lwt.2016.08.045>.
157. Ach, D.; Briançon, S.; Broze, G.; Puel, F.; Rivoire, A.; Galvan, J.-M.; Chevalier, Y. Formation of Microcapsules by Complex Coacervation. *Can. J. Chem. Eng.* **2015**, *93*, 183–191. <https://doi.org/10.1002/cjce.22086>.
158. Alexandre, J.D.B.; Barroso, T.L.C.T.; Oliveira, M.D.A.; Mendes, F.R.D.S.; Costa, J.M.C.D.; Moreira, R.D.A.; Furtado, R.F. Cross-Linked Coacervates of Cashew Gum and Gelatin in the Encapsulation of Pequi Oil. *Cienc. Rural* **2019**, *49*. <https://doi.org/10.1590/0103-8478cr20190079>.
159. Xia, Q.; Wang, B.; Akanbi, T.O.; Li, R.; Yang, W.; Adhikari, B.; Barrow, C.J. Microencapsulation of Lipase Produced Omega-3 Concentrates Resulted in Complex Coacervates with Unexpectedly High Oxidative Stability. *J. Funct. Foods* **2017**, *35*, 499–506. <https://doi.org/10.1016/j.jff.2017.06.017>.
160. Rocha-Selmi, G.A.; Bozza, F.T.; Thomazini, M.; Bolini, H.M.A.; Fávoro-Trindade, C.S. Microencapsulation of Aspartame by Double Emulsion Followed by Complex Coacervation to Provide Protection and Prolong Sweetness. *Food Chem.* **2013**, *139*, 72–78. <https://doi.org/10.1016/j.foodchem.2013.01.114>.

161. Calderón-Oliver, M.; Pedroza-Islas, R.; Escalona-Buendía, H.B.; Pedraza-Chaverri, J.; Ponce-Alquicira, E. Comparative Study of the Microencapsulation by Complex Coacervation of Nisin in Combination with an Avocado Antioxidant Extract. *Food Hydrocoll.* **2017**, *62*, 49–57. <https://doi.org/10.1016/j.foodhyd.2016.07.028>.
162. A.Bosnea, L.; Moschakis, T.; G.Biliaderis, C. Microencapsulated Cells of *Lactobacillus Paracasei* Subsp. *Paracasei* in Biopolymer Complex Coacervates and Their Function in a Yogurt Matrix. *Food Funct.* **2017**, *8*, 554–562. <https://doi.org/10.1039/C6FO01019A>.
163. Dolgin, E. What Lava Lamps and Vinaigrette Can Teach Us about Cell Biology. *Nature* **2018**, *555*, 300–302. <https://doi.org/10.1038/d41586-018-03070-2>.
164. Uversky, V.N. Protein Intrinsic Disorder-Based Liquid–Liquid Phase Transitions in Biological Systems: Complex Coacervates and Membrane-Less Organelles. *Adv. Colloid Interface Sci.* **2017**, *239*, 97–114. <https://doi.org/10.1016/j.cis.2016.05.012>.
165. Banani, S.F.; Lee, H.O.; Hyman, A.A.; Rosen, M.K. Biomolecular Condensates: Organizers of Cellular Biochemistry. *Nat. Rev. Mol. Cell Biol.* **2017**, *18*, 285–298. <https://doi.org/10.1038/nrm.2017.7>.
166. Deng, N.-N.; Huck, W.T.S. Microfluidic Formation of Monodisperse Coacervate Organelles in Liposomes. *Angew. Chem.* **2017**, *129*, 9868–9872. <https://doi.org/10.1002/ange.201703145>.
167. Drobot, B.; Iglesias-Artola, J.M.; Le Vay, K.; Mayr, V.; Kar, M.; Kreysing, M.; Mutschler, H.; Tang, T.-Y.D. Compartmentalised RNA Catalysis in Membrane-Free Coacervate Protocells. *Nat. Commun.* **2018**, *9*, 3643. <https://doi.org/10.1038/s41467-018-06072-w>.
168. Kojima, T.; Takayama, S. Membraneless Compartmentalization Facilitates Enzymatic Cascade Reactions and Reduces Substrate Inhibition. *ACS Appl. Mater. Interfaces* **2018**, *10*, 32782–32791. <https://doi.org/10.1021/acsami.8b07573>.
169. Qiao, Y.; Li, M.; Qiu, D.; Mann, S. Response-Retaliative Behavior in Synthetic Protocell Communities. *Angew. Chem.* **2019**, *131*, 17922–17927. <https://doi.org/10.1002/ange.201909313>.
170. Aumiller, W.M.; Keating, C.D. Experimental Models for Dynamic Compartmentalization of Biomolecules in Liquid Organelles: Reversible Formation and Partitioning in Aqueous Biphasic Systems. *Adv. Colloid Interface Sci.* **2017**, *239*, 75–87. <https://doi.org/10.1016/j.cis.2016.06.011>.
171. Cinar, S.; Cinar, H.; Chan, H.S.; Winter, R. Pressure-Sensitive and Osmolyte-Modulated Liquid–Liquid Phase Separation of Eye-Lens  $\gamma$ -Crystallins. *J. Am. Chem. Soc.* **2019**, *141*, 7347–7354. <https://doi.org/10.1021/jacs.8b13636>.
172. Schuster, B.S.; Reed, E.H.; Parthasarathy, R.; Jahnke, C.N.; Caldwell, R.M.; Bermudez, J.G.; Ramage, H.; Good, M.C.; Hammer, D.A. Controllable Protein Phase Separation and Modular Recruitment to Form Responsive Membraneless Organelles. *Nat. Commun.* **2018**, *9*, 2985. <https://doi.org/10.1038/s41467-018-05403-1>.
173. Banerjee, P.R.; Milin, A.N.; Moosa, M.M.; Onuchic, P.L.; Deniz, A.A. Reentrant Phase Transition Drives Dynamic Substructure Formation in Ribonucleoprotein Droplets. *Angew. Chem.* **2017**, *129*, 11512–11517. <https://doi.org/10.1002/ange.201703191>.
174. Martin, N.; Tian, L.; Spencer, D.; Coutable-Pennarun, A.; Anderson, J.L.R.; Mann, S. Photoswitchable Phase Separation and Oligonucleotide Trafficking in DNA Coacervate Microdroplets. *Angew. Chem.* **2019**, *131*, 14736–14740. <https://doi.org/10.1002/ange.201909228>.
175. Magana, J.R.; Sproncken, C.C.M.; Voets, I.K. On Complex Coacervate Core Micelles: Structure-Function Perspectives. *Polymers* **2020**, *12*, 1953. <https://doi.org/10.3390/polym12091953>.
176. Mohanty, B.; Aswal, V.K.; Kohlbrecher, J.; Bohidar, H.B. Synthesis of Gelatin Nanoparticles via Simple Coacervation. *J. Surf. Sci. Technol.* **2005**, *21*, 149–160.
177. Barthold, S.; Kletting, S.; Taffner, J.; Carvalho-Wodarz, C.D.S.; Lepeltier, E.; Loretz, B.; Lehr, C.-M. Preparation of Nanosized Coacervates of Positive and Negative Starch Derivatives Intended for Pulmonary Delivery of Proteins. *J. Mater. Chem. B* **2016**, *4*, 2377–2386. <https://doi.org/10.1039/C6TB00178E>.
178. Patra, S.; Basak, P.; Tibarewala, D.N. Synthesis of Gelatin Nano/Submicron Particles by Binary Nonsolvent Aided Coacervation (BNAC) Method. *Mater. Sci. Eng. C* **2016**, *59*, 310–318. <https://doi.org/10.1016/j.msec.2015.10.011>.
179. Awada, H.K.; Hwang, M.P.; Wang, Y. Towards Comprehensive Cardiac Repair and Regeneration after Myocardial Infarction: Aspects to Consider and Proteins to Deliver. *Biomaterials* **2016**, *82*, 94–112. <https://doi.org/10.1016/j.biomaterials.2015.12.025>.
180. Blocher, W.C.; Perry, S.L. Complex Coacervate-Based Materials for Biomedicine. *WIREs Nanomed. Nanobiotechnol.* **2017**, *9*, e1442. <https://doi.org/10.1002/wnan.1442>.
181. Park, U.; Lee, M.S.; Jeon, J.; Lee, S.; Hwang, M.P.; Wang, Y.; Yang, H.S.; Kim, K. Coacervate-Mediated Exogenous Growth Factor Delivery for Scarless Skin Regeneration. *Acta Biomater.* **2019**, *90*, 179–191. <https://doi.org/10.1016/j.actbio.2019.03.052>.
182. Johnson, N.R.; Kruger, M.; Goetsch, K.P.; Zilla, P.; Bezuidenhout, D.; Wang, Y.; Davies, N.H. Coacervate Delivery of Growth Factors Combined with a Degradable Hydrogel Preserves Heart Function after Myocardial Infarction. *ACS Biomater. Sci. Eng.* **2015**, *1*, 753–759. <https://doi.org/10.1021/acsbiomaterials.5b00077>.
183. Wang, Z.; Long, D.W.; Huang, Y.; Khor, S.; Li, X.; Jian, X.; Wang, Y. Fibroblast Growth Factor-1 Released from a Heparin Coacervate Improves Cardiac Function in a Mouse Myocardial Infarction Model. *ACS Biomater. Sci. Eng.* **2017**, *3*, 1988–1999. <https://doi.org/10.1021/acsbiomaterials.6b00509>.
184. Li, R.; Ma, J.; Wu, Y.; Nangle, M.; Zou, S.; Li, Y.; Yin, J.; Zhao, Y.; Xu, H.; Zhang, H.; et al. Dual Delivery of NGF and BFGF Coacervate Ameliorates Diabetic Peripheral Neuropathy via Inhibiting Schwann Cells Apoptosis. *Int. J. Biol. Sci.* **2017**, *13*, 640–651. <https://doi.org/10.7150/ijbs.18636>.

185. De Silva, U.K.; Brown, J.L.; Lapitsky, Y. Poly(Allylamine)/Triphosphosphate Coacervates Enable High Loading and Multiple-Month Release of Weakly Amphiphilic Anionic Drugs: An in Vitro Study with Ibuprofen. *RSC Adv.* **2018**, *8*, 19409–19419. <https://doi.org/10.1039/C8RA02588F>.
186. Zhang, Z.; Li, H.; Kasmi, S.; Van Herck, S.; Deswarte, K.; Lambrecht, B.N.; Hoogenboom, R.; Nuhn, L.; De Geest, B.G. A Synthetic, Transiently Thermoresponsive Homopolymer with UCST Behaviour within a Physiologically Relevant Window. *Angew. Int. Ed.* **2019**, *58*, 7866–7872. <https://doi.org/10.1002/anie.201900224>.
187. Nishida, K.; Tamura, A.; Yui, N. PH-Responsive Coacervate Droplets Formed from Acid-Labile Methylated Polyrotaxanes as an Injectable Protein Carrier. *Biomacromolecules* **2018**, *19*, 2238–2247. <https://doi.org/10.1021/acs.biomac.8b00301>.
188. Lim, Z.W.; Ping, Y.; Miserez, A. Glucose-Responsive Peptide Coacervates with High Encapsulation Efficiency for Controlled Release of Insulin. *Bioconjugate Chem.* **2018**, *29*, 2176–2180. <https://doi.org/10.1021/acs.bioconjchem.8b00369>.
189. Chenglong, W.; Shuhan, X.; Jiayi, Y.; Wencai, G.; Guoxiong, X.; Hongjing, D. Dextran-Based Coacervate Nanodroplets as Potential Gene Carriers for Efficient Cancer Therapy. *Carbohydr. Polym.* **2020**, *231*, 115687. <https://doi.org/10.1016/j.carbpol.2019.115687>.
190. Sun, Y.; Lau, S.Y.; Lim, Z.W.; Chang, S.C.; Ghadessy, F.; Partridge, A.; Miserez, A. Phase-Separating Peptides for Direct Cytosolic Delivery and Redox-Activated Release of Macromolecular Therapeutics. *Nat. Chem.* **2022**, *14*, 274–283. <https://doi.org/10.1038/s41557-021-00854-4>.
191. Jing, H.; Du, X.; Mo, L.; Wang, H. Self-Coacervation of Carboxymethyl Chitosan as a PH-Responsive Encapsulation and Delivery Strategy. *Int. J. Biol. Macromol.* **2021**, *192*, 1169–1177. <https://doi.org/10.1016/j.ijbiomac.2021.10.072>.